PLOS PATHOGENS

RESEARCH ARTICLE

Genetic targeting of *Card19* is linked to disrupted NINJ1 expression, impaired cell lysis, and increased susceptibility to *Yersinia* infection

Elisabet Bjanes[1,2¤a], Reyna Garcia Sillas[2], Rina Matsuda[1,2], Benjamin Demarco[3], Timothée Fettrelet[3], Alexandra A. DeLaney[1,2], Opher S. Kornfeld[4], Bettina L. Lee[4], Eric M. Rodríguez López[2,5], Daniel Grubaugh[2], Meghan A. Wynosky-Dolfi[2¤b], Naomi H. Philip[2,5¤c], Elise Krespan[2,6], Dorothy Tovar[2¤d], Leonel Joannas[2,7], Daniel P. Beiting[2,6,8], Jorge Henao-Mejia[8,9,10], Brian C. Schaefer[11], Kaiwen W. Chen[3¤e], Petr Broz[3], Igor E. Brodsky[1,2,5,8]*

1 Cell and Molecular Biology Graduate Group, University of Pennsylvania Perelman School of Medicine, Philadelphia, Pennsylvania, United States of America, 2 Department of Pathobiology, University of Pennsylvania School of Veterinary Medicine, Philadelphia, Pennsylvania, United States of America, 3 Department of Biochemistry, University of Lausanne, Epalinges, Vaud, Switzerland, 4 Department of Physiological Chemistry, Genentech Inc., South San Francisco, California, United States of America, 5 Immunology Graduate Group, University of Pennsylvania Perelman School of Medicine, Philadelphia, Pennsylvania, United States of America, 6 Center for Host Microbial Interactions, University of Pennsylvania School of Veterinary Medicine, Philadelphia, Pennsylvania, United States of America, 7 CRISPR/Cas9 Mouse Targeting Core, University of Pennsylvania School of Veterinary Medicine, Philadelphia, Pennsylvania, United States of America, 8 Institute for Immunology, University of Pennsylvania Perelman School of Medicine, Philadelphia, Pennsylvania, United States of America, 9 Department of Pathology and Laboratory Medicine, University of Pennsylvania, Philadelphia, Pennsylvania, United States of America, 10 Division of Protective Immunity, Department of Pathology and Laboratory Medicine, Children's Hospital of Philadelphia, University of Pennsylvania, Philadelphia, Pennsylvania, United States of America, 11 Department of Microbiology and Immunology, Uniformed Services University, Bethesda, Maryland, United States of America

¤a Current address: Department of Pediatrics, University of California San Diego, La Jolla, California, United States of America
¤b Current address: Immunology Research Unit, GlaxoSmithKline, Collegeville, Pennsylvania, United States of America
¤c Current address: Department of Immunobiology, Yale University School of Medicine, New Haven, Connecticut, United States of America
¤d Current address: Department of Microbiology & Immunology, Stanford University School of Medicine, Palo Alto California, United States of America
¤e Current address: Immunology Programme and Department of Microbiology & Immunology, Yong Loo Lin School of Medicine, National University of Singapore, Singapore
* ibrodsky@vet.upenn.edu

Abstract

Cell death plays a critical role in inflammatory responses. During pyroptosis, inflammatory caspases cleave Gasdermin D (GSDMD) to release an N-terminal fragment that generates plasma membrane pores that mediate cell lysis and IL-1 cytokine release. Terminal cell lysis and IL-1β release following caspase activation can be uncoupled in certain cell types or in response to particular stimuli, a state termed hyperactivation. However, the factors and mechanisms that regulate terminal cell lysis downstream of GSDMD cleavage remain poorly understood. In the course of studies to define regulation of pyroptosis during *Yersinia*

infection, we identified a line of *Card19*-deficient mice (*Card19^{Ixcn}*) whose macrophages were protected from cell lysis and showed reduced apoptosis and pyroptosis, yet had wild-type levels of caspase activation, IL-1 secretion, and GSDMD cleavage. Unexpectedly, CARD19, a mitochondrial CARD-containing protein, was not directly responsible for this, as an independently-generated CRISPR/Cas9 *Card19* knockout mouse line (*Card19^{Null}*) showed no defect in macrophage cell lysis. Notably, *Card19* is located on chromosome 13, immediately adjacent to *Ninj1*, which was recently found to regulate cell lysis downstream of GSDMD activation. RNA-seq and western blotting revealed that *Card19^{Ixcn}* BMDMs have significantly reduced NINJ1 expression, and reconstitution of *Ninj1* in *Card19^{Ixcn}* immortalized BMDMs restored their ability to undergo cell lysis in response to caspase-dependent cell death stimuli. *Card19^{Ixcn}* mice exhibited increased susceptibility to *Yersinia* infection, whereas independently-generated *Card19^{Null}* mice did not, demonstrating that cell lysis itself plays a key role in protection against bacterial infection, and that the increased infection susceptibility of *Card19^{Ixcn}* mice is attributable to loss of NINJ1. Our findings identify genetic targeting of *Card19* being responsible for off-target effects on the adjacent gene *Ninj1*, disrupting the ability of macrophages to undergo plasma membrane rupture downstream of gasdermin cleavage and impacting host survival and bacterial control during *Yersinia* infection.

Author summary

Programmed cell death is critical for regulating tissue homeostasis and host defense against infection. Pyroptosis is an inflammatory form of programmed cell death that couples cell lysis with release of inflammatory cytokines. Cell lysis is triggered by activation of particular intracellular pore forming proteins, but how regulation of cell lysis occurs is not well understood. Genetic targeting of *Card19* on chromosome 13 resulted in decreased expression of the adjacent gene, *Ninj1*, which was recently found to regulate terminal lysis events in response to cell death-inducing stimuli. Consistently, macrophages from *Card19*-deficient mice were resistant to multiple forms of cell death in response to a variety of inflammatory stimuli, including canonical and non-canonical inflammasome activation, as well as triggers of cell-extrinsic apoptosis. Notably, *Card19*-deficient mice were more susceptible to *Yersinia* infection, indicating that cell lysis contributes to control of bacterial infections. Our data provide new insight into the impact of terminal cell lysis on control of bacterial infection and highlight the role of additional factors that regulate lytic cell death downstream of gasdermin cleavage.

Introduction

Regulated cell death is an evolutionarily conserved mechanism by which multicellular organisms control fundamental biological processes ranging from tissue development to microbial infection. Apoptosis and pyroptosis represent two distinct forms of regulated cell death that are activated in response to diverse stimuli, including developmental signals [1,2], tissue stress or injury [3], and microbial infection [4–7]. While apoptosis is an immunologically quiescent or suppressive form of cell death during tissue homeostasis and development, certain stimuli, including infections and chemotherapeutic agents, induce apoptosis that is accompanied by

inflammatory signals that contribute to anti-pathogen and anti-tumor immunity [8–10]. Apoptosis is activated by specific apoptotic initiator caspases, following certain intrinsic or extrinsic signals, and mediates organized disassembly of the cell via a process that limits cellular permeability and enables phagocytosis of the dying cell [11,12]. Alternatively, pyroptosis is a lytic form of regulated cell death characterized by caspase-1- or -11-dependent plasma membrane disruption mediated by cleavage and activation of the pore forming protein Gasdermin D (GSDMD), and release of interleukin-1 (IL-1) family cytokines and other intracellular components [13–16]. However, inhibition of the receptor-proximal signaling kinases TAK1 or IKK by chemotherapeutic drugs or during infection by bacterial pathogens such as *Yersinia*, can trigger a caspase-8-dependent apoptosis pathway that is also associated with GSDMD cleavage [17–19]. Interestingly, a recent study demonstrated that only caspase-8 activated in the RIPK1-containing complex IIb can efficiently cleave GSDMD in macrophages [20]. These findings suggest a potential point of intersection of cell death pathways previously viewed as distinct [21].

During pyroptosis, secretion of IL-1 family cytokines and release of intracellular contents are temporally and genetically linked, and it has been suggested that IL-1 cytokines are released from cells when they undergo caspase-1 or -11-dependent lysis [22,23]. However, IL-1 secretion and cell lysis can be uncoupled in certain cell types or in response to specific stimuli. For example, the osmoprotectant glycine prevents release of lactate dehydrogenase (LDH), a key indicator of cell lysis, but does not affect IL-1β cytokine release [24,25]. Conversely, genetic ablation of IL-1 does not prevent cell lysis following pyroptotic stimuli. Moreover, IL-1 secretion can occur by living cells in the absence of apparent cytotoxicity [26,27]. Notably, neutrophils and monocytes display evidence of caspase-1 processing and IL-1 secretion in the absence of cell lysis [28,29]. Furthermore, dendritic cells treated with the oxidized lipid oxPAPC, or macrophages treated with the *N*-acetyl glucosamine fragment of bacterial peptidoglycan, release IL-1 without undergoing cell death [30,31]. Interestingly, GSDMD is genetically required for the release of IL-1 cytokines in response to non-pyroptotic stimuli, a state termed hyperactivation [26,31,32]. Collectively, these data imply that while GSDMD processing and membrane insertion are critical for ultimate cell lysis, a cell fate decision checkpoint exists that distinguishes GSDMD-dependent IL-1 secretion from terminal cell death.

In our efforts to identify regulators of cell death during bacterial infection, we investigated the caspase activation and recruitment domain (CARD)-containing protein CARD19 [33]. CARD19 is a mitochondrial membrane protein that contains an N-terminal CARD and C-terminal transmembrane domain, suggesting that it could be involved in the regulation of cell death or inflammatory responses [33,34]. Multiple mitochondria-associated proteins regulate inflammasome activation and inflammatory signaling [35–37]. Notably, the mitochondrial CARD-containing protein, MAVS, plays a critical role in anti-viral immune signaling and IL-1 cytokine release [35,38], and the mitochondrial outer membrane lipid cardiolipin plays an important role in regulating NLRP3 inflammasome assembly [39].

Intriguingly, primary macrophages from *Card19*-deficient mice (*Card19^lxcn*) were resistant to cell lysis and release of lytic cell markers in response to apoptotic and pyroptotic stimuli, but exhibited wild-type levels of caspase activation, IL-1 secretion, and gasdermin processing. Unexpectedly however, two independent CRISPR/Cas9 knockout mouse lines that we generated did not show the same phenotype; furthermore, expression of CARD19 in immortalized BMDMs from the original *Card19^lxcn* line did not restore their ability to undergo lysis, indicating that CARD19 itself is unlikely to be responsible for regulating terminal cell lysis in response apoptotic and pyroptotic stimuli. The cell lysis defect in *Card19^lxcn* mice was unrelated to Sterile alpha and heat armadillo motif-containing protein (SARM1), which was reported to regulate NLRP3 inflammasome-dependent cell death independently of IL-1β cytokine release [40], as BMDMs from four independent *Sarm1^-/-* lines showed no defects in cell

death, IL-1β release, and GSDMD cleavage. RNA-seq identified a handful of differentially regulated genes in *Card19^{lxcn}* BMDMs, including a recently reported regulator of plasma membrane lysis, *Ninj1* [41], which is located adjacent to *Card19* on chromosome 13. Notably, *Card19^{lxcn}* BMDMs showed significantly reduced *Ninj1* mRNA expression at baseline and diminished NINJ1 protein levels both at baseline and upon LPS stimulation. Critically, reconstitution of immortalized *Card19^{lxcn}* BMDMs rescued the defect in cell lysis, similar to *Ninj1^{-/-}* BMDMs, indicating that the phenotype of *Card19^{lxcn}* mice results from a defect in NINJ1 protein expression. *Card19^{lxcn}* mice were more susceptible to infection with *Yersinia*, exhibiting enhanced mortality and systemic bacterial burdens relative to wildtype mice, implicating NINJ1-mediated lysis in host-pathogen interactions. Our data extend recent findings describing NINJ1 as a regulator of cell lysis downstream of caspase activation and gasdermin cleavage, and highlight the role of lytic cell death in host defense against bacterial infection.

Results

Card19^{lxcn} BMDMs are deficient for caspase-dependent cell death

Our efforts to understand how cell death is regulated during bacterial infection led us to investigate the mitochondrial CARD-containing protein, CARD19, formerly known as BinCARD-2 [33,34]. To test the possible contribution of CARD19 to cell death during pyroptosis, we compared the kinetics of cell death in primary bone marrow derived macrophages (BMDMs) from B6 mice and mice with a targeted deletion in *Card19* generated by Lexicon Genetics (designated *Card19^{lxcn}*), in response to infection by *Salmonella enterica* serovar Typhimurium (*S.* Tm) or LPS +ATP treatment. *S.* Tm infection of BMDMs activates the well-characterized NAIP/NLRC4/caspase-1 inflammasome pathway, leading to pyroptosis and IL-1 cytokine release [4,5,42,43]. In contrast, LPS+ATP treatment activates the NLRP3/ASC/caspase-1 inflammasome, which induces pyroptosis and IL-1 cytokine release via activation of the P2X7 receptor and potassium efflux [44–48]. *Card19^{lxcn}* BMDMs displayed a striking and significant defect in cell death following *S.* Tm infection or LPS+ATP treatment, as measured by release of LDH (**Figs 1A, 1B and S1A and S1B**). Consistently, *Card19^{lxcn}* BMDMs exhibited significantly reduced levels of membrane permeability as determined by PI uptake, both in kinetics and amplitude (**Fig 1C and 1D**).

Card19^{lxcn} BMDMs also exhibited a significant defect in cell death following infection by *Yersinia pseudotuberculosis* (*Yptp*), which activates cell-extrinsic caspase-8- and RIPK1-dependent apoptosis in response to *Yptb* blockade of IKK- and MAPK-signaling [6,49,50], as well as in response to staurosporine (Sts), a broad-spectrum kinase inhibitor that induces cell-intrinsic apoptosis and also activates caspase-8 in myeloid cells [51–53] (**Fig 1E and 1F**). These observations were also mirrored by delayed PI uptake in *Card19^{lxcn}* BMDMs (**Fig 1G and 1H**). Strikingly, *Card19^{lxcn}* BMDMs were resistant to cell death in response to multiple apoptotic and pyroptotic stimuli, including cycloheximide, etoposide, and noncanonical inflammasome activation (**Fig 2A–2C**). However, RIPK3-dependent programmed necrosis which occurs in response to LPS and the pan-caspase inhibitor z-VAD-FMK [54,55], was unaffected by CARD19-deficiency (**Fig 2D**). Altogether, these findings demonstrate that BMDMs from *Card19^{lxcn}* mice exhibit increased resistance to membrane permeability and terminal cell lysis downstream of apoptotic and pyroptotic triggers.

Peritoneal macrophages from *Card19^{lxcn}* mice have reduced levels of cell death

The peritoneal cavity contains two distinct populations of macrophages, termed Large and Small (LPM and SPM, respectively) [56]. At baseline, the primary population is the LPM,
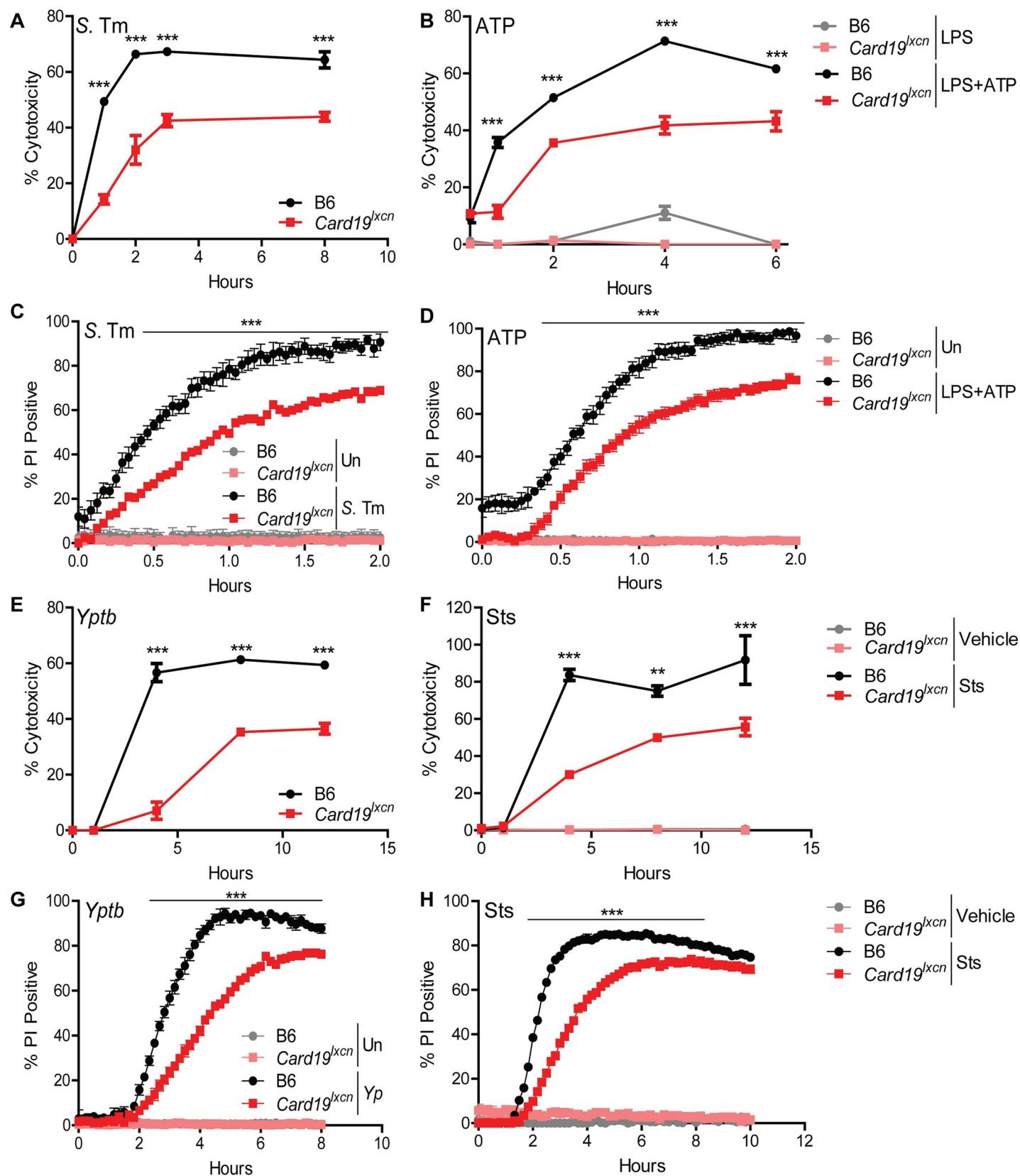
Fig 1. *Card19^{lxcn}* BMDMs are deficient for caspase-dependent cell death. Primary C57BL/6J (B6) or *Card19^{lxcn}* BMDMs were infected with *Salmonella enterica* serovar Typhimurium (*S.* Tm) or *Y. pseudotuberculosis* (*Yptb*), or treated with LPS+ATP or staurosporine (Sts), as indicated, and the kinetics of cell death was assayed by release of lactate dehydrogenase (LDH) (A, B, E, F) or propidium iodide (PI) uptake (C, D, G, H). Each figure is representative of three or more independent experiments. LDH release was assayed at specific times post-infection. PI uptake was measured over a two or ten-hour timecourse with fluorometric measurements taken at 2.5 minute (C, D) or 10 minute (G, H) intervals. Mean ± SEM of triplicate wells is displayed. Each panel is representative of three or more independent experiments. *** p < 0.001, ** p < 0.01, * p < 0.05. n.s. not significant, analyzed by 2-way ANOVA with Bonferroni multiple comparisons post-test.

while 2 days post-injection of LPS or other inflammatory triggers, such as thioglycolate, the primary population in the peritoneal cavity shifts to the SPM [56,57]. Interestingly, thioglycolate-elicited peritoneal macrophages exhibited significantly higher levels of LDH than peritoneal macrophages isolated from PBS-treated mice following infection with either *S.*Tm or *Yptb* (**Fig 3A–3C**). These data indicate that SPM undergo elevated levels of cell death relative to LPMs. Moreover, thioglycolate-elicited PMs from *Card19^{lxcn}* mice had significantly lower levels of LDH release that C57BL/6J PMs. It is possible that the results could be explained by a defect in SPMs in *Card19^{lxcn}* mice following thioglycolate treatment; however, these results are consistent with our findings in primary BMDMs that *ex vivo* isolated macrophages from *Card19^{lxcn}* animals also have a defect in cell lysis (**Fig 3D and 3E**).
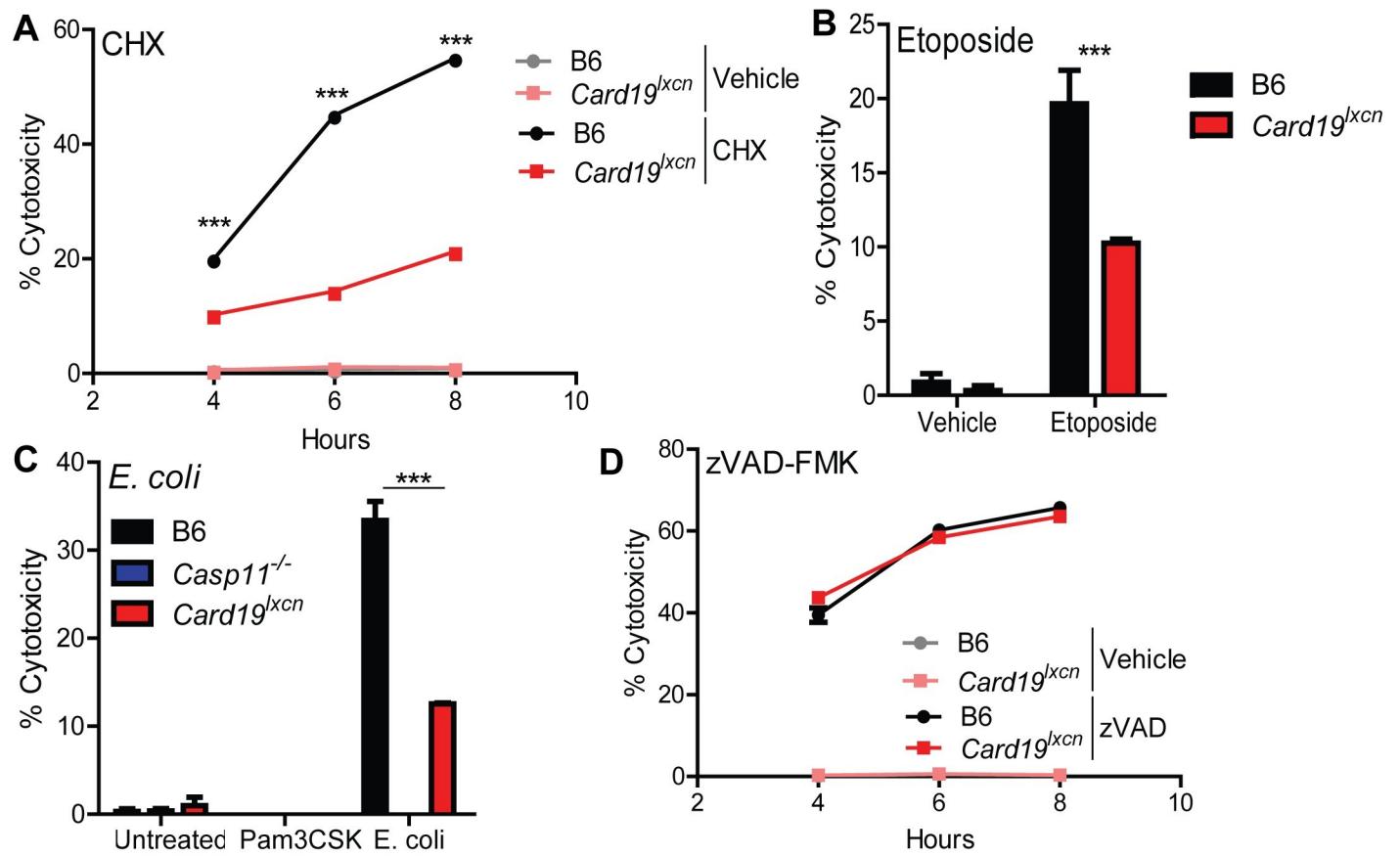
Fig 2. *Card19^{lxcn}* BMDMs are deficient in apoptosis and non-canonical inflammasome-induced pyroptosis but not necroptosis. Primary C57BL/6J (B6), *Card19^{lxcn}*, *Card19$^{+/+}$*, and *Casp11$^{-/-}$* BMDMs were treated with (A) Cycloheximide (CHX) (B) etoposide, (C) Pam3CSK+*E. coli* or (D) z-VAD-FMK + LPS and cell death was assayed by LDH release. BMDMs were treated, supernatants were harvested from triplicate wells at (A) (D) indicated time points (B) 24 hours, or (C) 16 hours and measured for cytotoxicity. Mean ± SEM of triplicate wells is displayed. Each figure is representative of 2 or more independent experiments. *** p < 0.001, ** p < 0.01, * p < 0.05. n.s. not significant. 2-way ANOVA with Bonferroni multiple comparisons post-test.
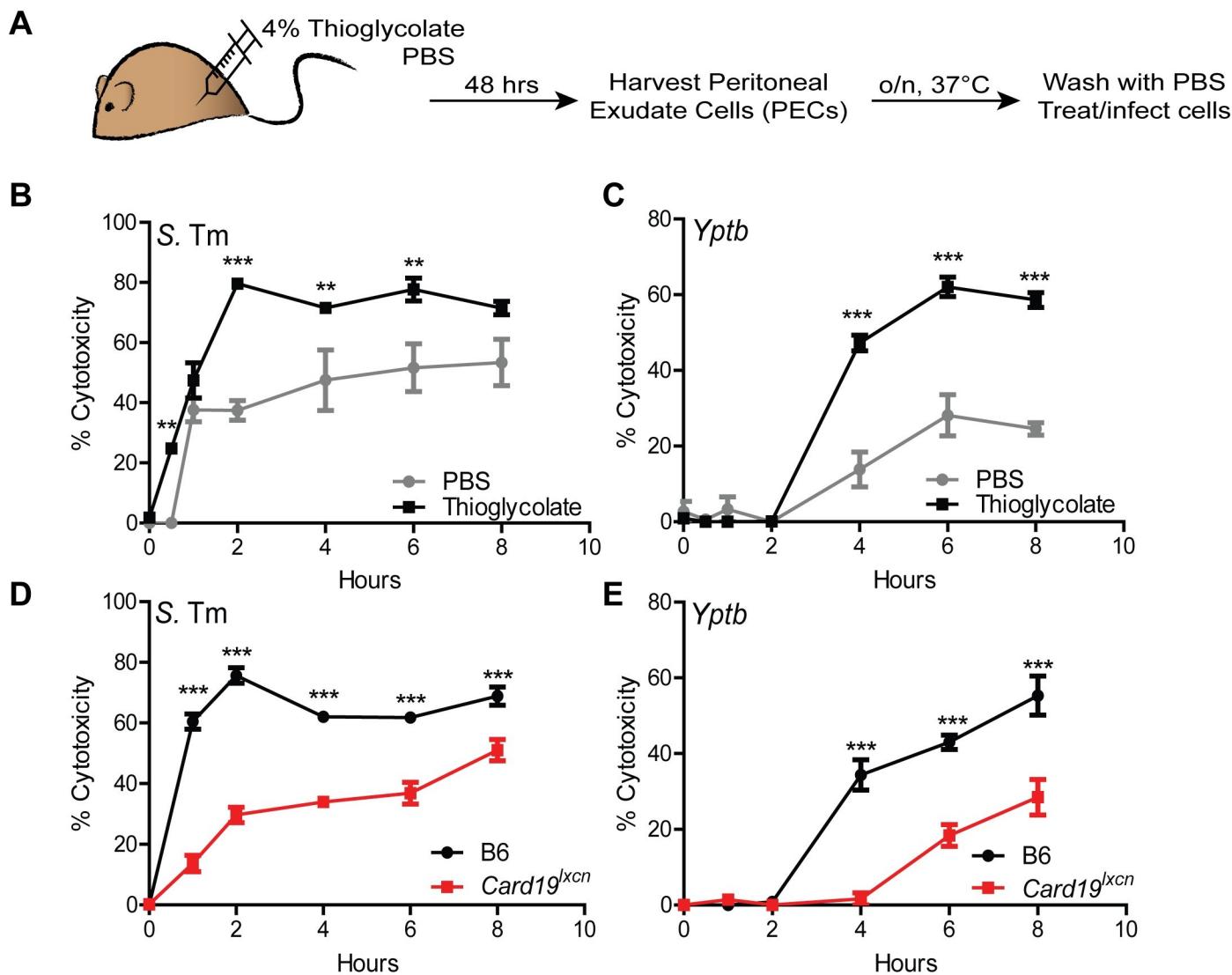
Fig 3. Peritoneal macrophages from *Card19^{lxcn}* mice have reduced levels of cell death. (A) B6 and *Card19^{lxcn}* mice were injected with 4% aged thioglycolate or PBS. 48 hrs later, PECS were harvested, RBC lysed, counted and plated in triplicate overnight at 37˚C. PBS PECS were pooled prior to plating. Cells were washed with PBS to remove non-adherent cells and infected with *Yptb* or *S*. Tm (MOI 10) or treated with staurosporine (10 uM). Cytotoxicity was measured by LDH release at indicated time points. *** p < 0.001, ** p < 0.01, * p < 0.05. n.s. not significant. 2-way ANOVA with Bonferroni multiple comparisons post-test. Graphs are representative of two independent experiments with 3–6 mice per group, per genotype. (B, C) PBS: mean ± SEM for technical replicates of 3 pooled B6 mice. Thioglycolate: means of technical replicates for 3 B6 mice ± SEM. Cells were infected with (B) *S*. Tm or (C) *Yptb*. (D, E) PBS: mean ± SEM for technical replicates of 4–6 pooled B6 and *Card19^{lxcn}* mice + SEM. Thioglycolate: means of technical replicates for 4 B6 and *Card19^{lxcn}* mice ± SEM. Cells were infected with (B) *S*. Tm or (C) *Yptb*.

https://doi.org/10.1371/journal.ppat.1009967.g003

Card19^{lxcn} BMDMs retain intracellular alarmin HMGB1 following activation of cell death

HMGB1 is a nuclear chromatin-associated protein that is released from cells upon loss of plasma membrane integrity [58]. As expected in B6 cells, *S*. Tm or LPS+ATP treatment led to significant HMGB1 release into the supernatant by one-hour post-infection, and by 4 hours post-exposure to *Yptb* or staurosporine (Sts) (**Fig 4A**). In contrast, *Card19^{lxcn}* cells exhibited significantly delayed release of HMGB1 for each respective timepoint, consistent with our findings that they exhibit increased resistance to membrane rupture (**Fig 4A**). HMGB1 was

virtually undetectable in *Card19^lxcn* macrophage supernatants one-hour post-treatment with *S.* Tm or LPS+ATP, and minimally detectable at 4 hours post-treatment in response to *Yptb* or Sts (**Fig 4A**). To obtain insight into the dynamics of HMGB1 release from cells, we analyzed HMGB1 release by confocal microscopy following exposure of Wt and *Card19^lxcn* cells to Sts. We observed three morphologies of HMGB1 staining–nuclear, in which the majority of HMGB1 was located in the nucleus; cellular, in which HMGB1 was absent from the nucleus but still contained within the confines of a cell; and extracellular, in which a cloud of HMGB1 was detectable surrounding what was likely the remnants of apoptotic cells and cellular debris. Notably, and consistent with intracellular retention of HMGB1 in *Card19^lxcn* cells, a higher frequency of *Card19*^lxcn cells relative to B6 BMDMs retained nuclear HMGB1 (**Fig 4B and 4C**), while B6 BMDMs exhibited extracellular HMGB1 cloud formation much more frequently than *Card19^lxcn* BMDMs (**Fig 4B white arrows and quantified in Fig 4D**). Altogether, these findings indicate that *Card19^lxcn* BMDMs resist cell lysis and release of intracellular contents during induction of cell death triggered by caspase-1 or caspase-8.

Card19^lxcn macrophages are not deficient in activation of caspase-1 or -8

Most currently known regulators of cell death act at the level of caspase activation or assembly of caspase-activating inflammasome complexes [59]. Pyroptosis is mediated by activation of caspase-1 or -11 [15,59,60], which cleave Gasdermin D (GSDMD), thereby triggering cell lysis by enabling formation of oligomeric N-terminal GSDMD pores in the plasma membrane [14,16,61,62]. Surprisingly, despite the significant reduction in cytotoxicity in *Card19^lxcn* cells, processing of caspase-1 was equivalent in B6 and *Card19^lxcn* cells 15 minutes post-infection, at which time cell death is virtually undetectable in either genotype (**Fig 5A**). Moreover, B6 cells released significant amounts of cleaved and pro-caspase-1 into cell supernatants at later time-points, in contrast to *Card19^lxcn* BMDMs (**Fig 5A**), consistent with the reduced levels of pyroptosis in *Card19^lxcn* cells in response to *S.* Tm infection. Reduced levels of cleaved caspase-1 in *Card19^lxcn* BMDM supernatants was matched by increased amounts of cleaved caspase-1 in *Card19^lxcn* whole cell lysates (**Fig 5A**). Similarly, initial processing of GSDMD to the cleaved p30 form was equivalent in B6 and *Card19^lxcn* cell lysates, while the release of processed GSDMD into the supernatant was significantly reduced in *Card19^lxcn* cells (**Fig 5A**). Thus, *Card19^lxcn* cells have no defect in either caspase-1 activation, or in the cleavage of caspase-1 targets.

Cell-extrinsic apoptosis is mediated by oligomerization and auto-processing of caspase-8 [63,64]. Active caspase-8 directly cleaves its pro-apoptotic downstream targets, including the Bcl-2 family member Bid [65,66], and the executioner caspases-3 and -7. Similarly to caspase-1, cleavage of caspase-8 as well as the processing of caspase-8 substrates, including Bid, caspase-3, the caspase-3 target poly-ADP ribose polymerase (PARP), and the pore-forming protein GSDME also known as DFNA5 [18,67], were equivalent in B6 and *Card19^lxcn* cells in response to *Yptb* infection or staurosporine treatment (**Fig 5B and 5C**). Notably, we observed GSDMD processing in response to *Yptb* infection as well as Sts treatment, in both B6 and *Card19^lxcn* BMDMs (**Fig 5C**). Importantly, direct comparison of caspase-1 and GSDMD processing in response to multiple stimuli revealed that *Card19^lxcn* cells had reduced release of cleaved caspase-1 and N-terminal GSDMD into the supernatant, and correspondingly increased retention in cell lysates, consistent with reduced terminal lysis of the cells in the absence of CARD19 (**Fig 5D**). *Card19^lxcn* BMDMs had wild-type levels of caspase-8 activity in response to either *Yptb* infection or Sts treatment, confirming that *Card19^lxcn* BMDM do not have a defect in caspase activity (**Fig 5E**). Altogether, these findings demonstrate that *Card19^lxcn* BMDMs do not have a defect in caspase activation or downstream target cleavage, and therefore likely have a defect in cell lysis downstream of caspase activation.
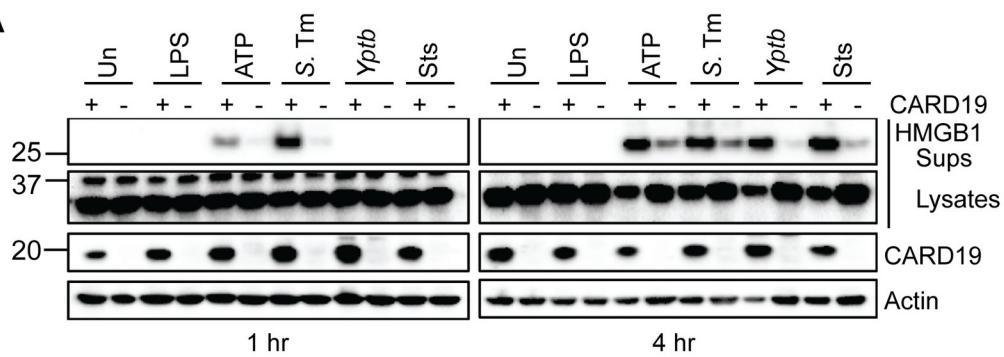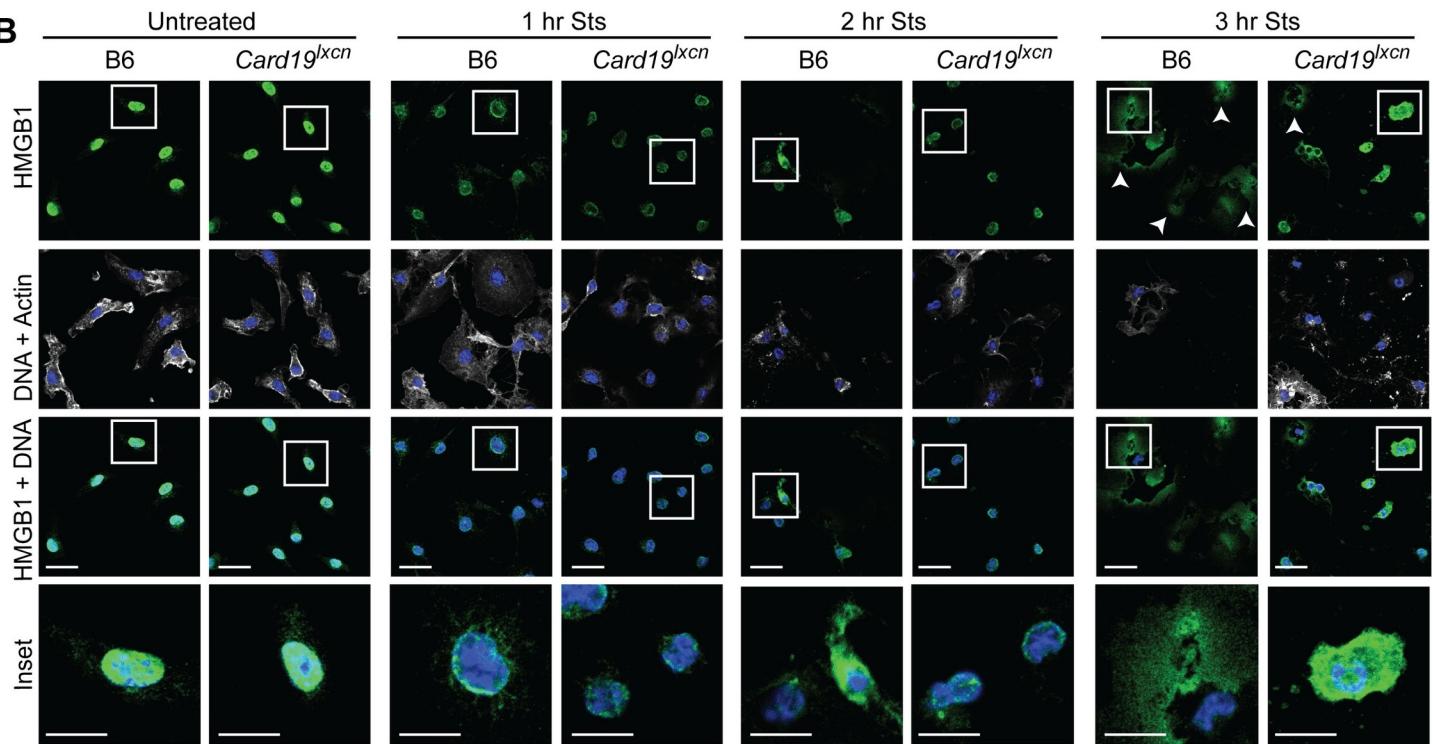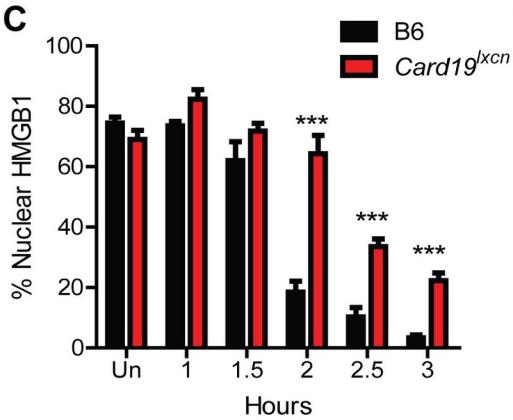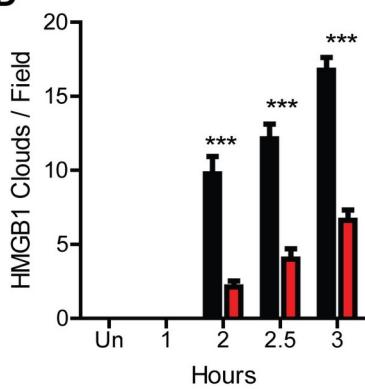
Fig 4. *Card19^lxcn* BMDMs retain intracellular alarmin HMGB1 following activation of cell death. (A) Primary BMDMs from B6 (+) or *Card19^lxcn* (-) mice were treated with indicated treatments or infections, and TCA precipitated supernatants (Sups) or whole cell lysates (Lysates) were harvested at 1 or 4 hours post-infection and analyzed by western blotting for HMGB1, CARD19, and actin (loading control). ATP indicates cells that were primed with LPS for 3 hours and treated with ATP for 1 or 4 hours. *S.Tm–Salmonella* Typhimurium; *Yptb Yersinia pseudotuberculosis*. Sts–staurosporine. (B) Confocal microscopy images of untreated and staurosporine (Sts) treated

B6 and *Card19*^{lxcn} BMDMs fixed at indicated times post-Sts treatment and stained for HMGB1, Actin and DNA (Hoescht). White arrows indicate HMGB1 clouds. Scale bar 20 microns, inset 10 microns. (C) Quantification of nuclear HMGB1. n = 25–50 cells per field, 5–8 fields per condition, per timepoint. (D) Quantification of HMGB1 clouds in B6 and *Card19*^{lxcn} BMDMs after staurosporine treatment. 5–8 fields quantified per condition, per timepoint. Mean ± SEM is displayed. *** p < 0.001, ** p < 0.01, * p < 0.05. n.s. not significant. 2-way ANOVA with Bonferroni multiple comparisons post-test. Representative of 3 (A-C) or 2 (D) independent experiments.

How *Card19*^{lxcn} cells might retain membrane integrity downstream of both inflammatory and apoptotic caspase activation is not clear. However, caspase-8 and caspase-1 can both cleave IL-1β [51,68,69], as well as GSDMD [17,18,20] raising the question of whether *Card19*^{lxcn} cells and *Gsdmd*^{-/-} cells have similar defects in cell lysis in response to *Yptb* infection. Surprisingly, although *Gsdmd*^{-/-} BMDMs exhibited a significant defect in cell death in response to *Yptb* infection (**S2A Fig**), this defect was not as pronounced as in *Card19*^{lxcn} BMDMs, suggesting that *Card19*^{lxcn} cells likely have a defect in additional GSDMD-independent mechanisms of cell lysis, potentially involving GSDME/DFNA5, which was also processed in response to *Yptb* infection (**S2B and S2C Fig**). Consistent with recent findings [17–19], we observed cleaved GSDMD in *Casp1/11*^{-/-} lysates following either *Yptb* infection or staurosporine treatment. Although levels of cleaved GSDMD were significantly lower than in Wt cells, this finding is consistent with findings that caspase-8 cleaves GSDMD less efficiently than caspase-1 (**S2B and S2C Fig**) [19]. The caspase-8-selective inhibitor, IETD, abrogated GSDMD and GSDME cleavage in response to *Yptb* or staurosporine (**S2B and S2C Fig**), suggesting that *Yersinia* and staurosporine induce GSDMD and GSDME cleavage in *Casp1/11*^{-/-} cells in a caspase-8-dependent manner. Consistently, *Ripk3*^{-/-} BMDMs showed robust cleavage of GSDMD and GSMDE while *Ripk3*^{-/-}*Casp8*^{-/-} BMDMs showed a near-complete absence of N-terminal GSDMD and GSDME p30 following *Yptb* infection and significant reduction in GSDMD and GSDME processing after staurosporine treatment (**S2B and S2C Fig**). Notably, caspase-1 activity was not defective in the *Ripk3*^{-/-}*Casp8*^{-/-} BMDMs (**S2D Fig**).

The cell death defect in *Card19*^{lxcn} BMDMs is independent from cytokine release

Consistent with our findings that *Card19*^{lxcn} BMDMs are not defective in their ability to regulate proteolytic activity of caspase-1, CARD19-deficient cells released wild-type levels of IL-1 cytokines in response to *S.* Tm, LPS+ATP, or infection with the Δ*yopEJK Yptb* strain, which triggers a caspase-11/NLRP3-dependent pathway of IL-1 cytokine release [70,71] (**Fig 6A and 6B**). These data indicate that *Card19*^{lxcn} cells most likely do not have a defect at the level of GSDMD-dependent pore formation and cytokine release, and that the *Card19*^{lxcn} cells decouple secretion of IL-1β from pyroptosis, which normally occurs in response to these stimuli [26,32]. Consistent with a recent finding that *Card19*^{lxcn} cells do not have altered NF-κB activation [33], *Card19*^{lxcn} BMDMs did not have a defect in secretion of IL-6, TNF, or IL-12p40, (**Fig 6C–6E**). Altogether, these findings suggest that *Card19*^{lxcn} cells have decoupled cell lysis as determined by LDH and HMGB1 release and the release of caspase-1-dependent cytokines.

Cells can release IL-1β while remaining viable during a state known as hyperactivation [26,32,72]. GSDMD is required for IL-1β secretion during hyperactivation, but the mechanism by which GSDMD mediates this IL-1β release without inducing lysis is not understood [26,72]. *Staphylococcus aureus* lacking OatA induces hyperactivation [26,72]. Despite inducing robust IL-1β release under conditions of minimal LDH release, Δ*oatA S. aureus*-infected B6 BMDM exhibited minimal levels of caspase-1 and GSDMD processing (**Fig 6F–6H**). CARD19 expression did not correlate with differences in hyperactivation exhibited between untreated, Δ*oatA* and *S.* Tm-infected BMDMs (**Fig 6F**). Since *Card19*^{lxcn} BMDMs process caspase-1 and GSDMD normally while releasing IL-1 cytokines in the absence of overt lysis, these data
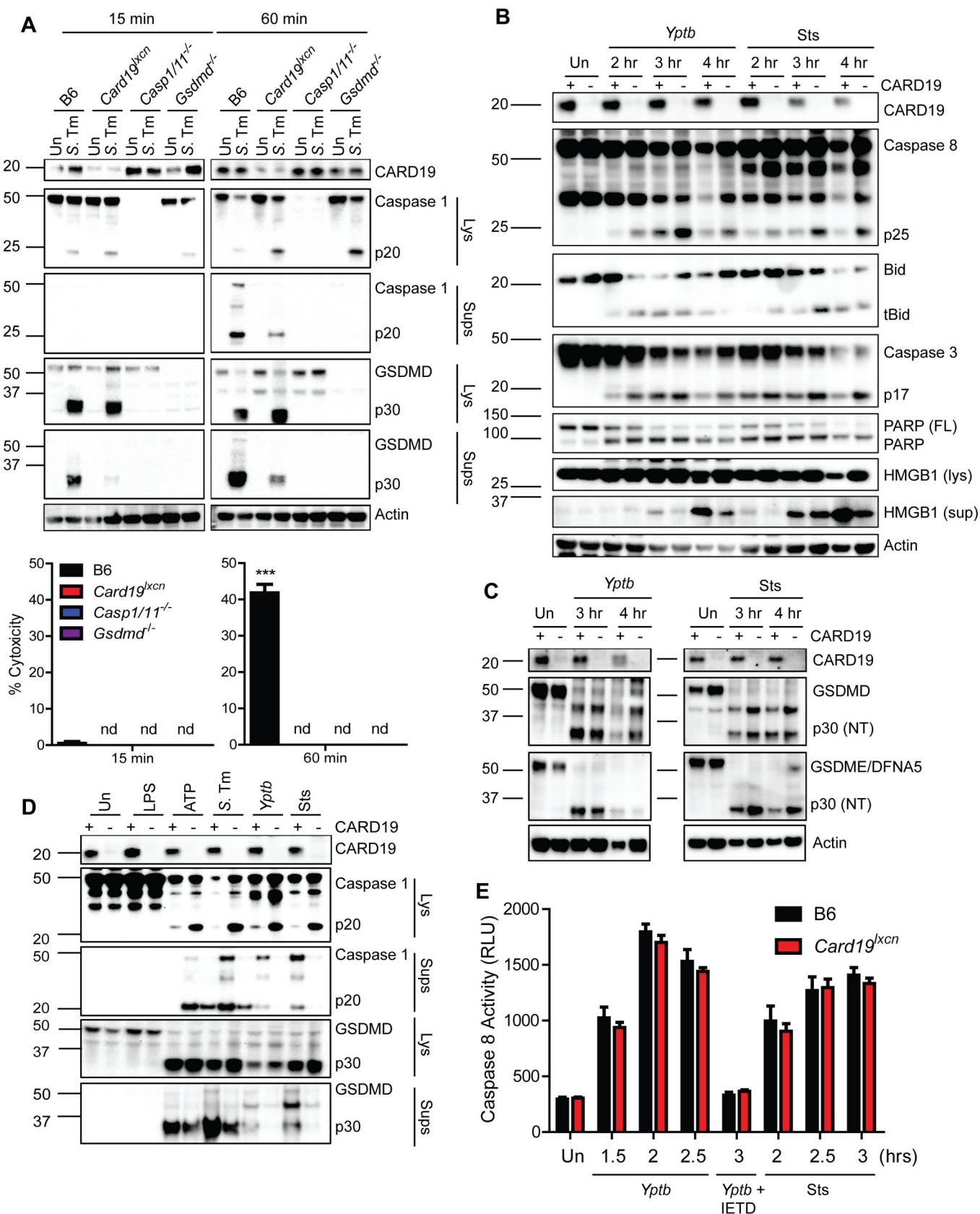
Fig 5. *Card19^lxcn* macrophages are not deficient in activation of caspase-1 or -8. (A) B6, *Card19^lxcn*, *Casp1/11^-/-* or *Gsdmd^-/-* BMDMs were left untreated or infected with *S.* Tm, and cell lysates (Lys) and TCA-precipitated supernatants (Sups) were run on SDS-PAGE and analyzed by western blotting for cleaved Casp1, GSDMD, or Actin (cell lysate loading control). Cell death from these cells was assayed in parallel by LDH release (indicated below blots). Mean ± SEM is displayed. 2-way ANOVA with Bonferroni multiple comparisons post-test. *** p < 0.001, ** p < 0.01, * p < 0.05. n.d. not detectable. (B) B6 (+) or *Card19^lxcn* (-) BMDMs were infected with *Yptb* or treated with Sts or 2, 3, or 4 hours, or left untreated (Un) as indicated. Cell lysates and TCA-supernatants (HMGB1 sup) were prepared at indicated times and analyzed for presence of CARD19, cleaved caspase-8, tBid, cleaved caspase-3, cleaved PARP, HMGB1 and Actin (loading control). (C) B6 and *Card19^lxcn* BMDMs were left untreated, infected with *Yptb* or treated with staurosporine. Lysates were harvested at the indicated time points, run on SDS-PAGE and analyzed by western blotting for CARD19, GSDMD, GSDME/DFNA5, and actin (loading control). (D) B6 (+) and *Card19^lxcn* (-) BMDMs were left untreated, treated with LPS, LPS+ATP, Sts, or infected with *S.* Tm or *Yptb*. Cell lysates (Lys) and supernatants (Sups) were harvested 1 hour post-ATP or S.Tm infection or 3 hours post Sts treatment and *Yptb* infection and assayed for CARD19, Caspase-1, and presence of cleaved GSDMD. (E) B6 and *Card19^lxcn* BMDMs were left untreated, infected with *Yptb*, or treated with staurosporine. BMDMs were pretreated with the caspase-8 inhibitor IETD for one hour prior to infection. Caspase-8 activity was assessed by Caspase-8-Glo. Mean ± SEM is displayed. Blots, caspase-8 activity and LDH are representative of at least 3 independent experiments.

indicate that lack of death in *Card19^lxcn* cells is not evidence of a hyperactivation phenotype, but suggests *Card19^lxcn* BMDMs are likely resistant to cell lysis due to a defect at a terminal stage of pyroptosis. Curiously, Δ*oatA*-infected cells exhibited significantly lower levels of GSDMD processing, indicating that threshold levels of GSDMD processing or membrane insertion may underlie the distinction between hyperactivation and cell lysis (**Fig 6F**).

Card19^lxcn BMDMs are hypomorphic for *NINJ1* gene and protein expression

Numerous mitochondrial proteins have been implicated in recent years as essential regulators of caspase activity, GSDMD and terminal events in during lysis [35,37,73]. While these studies were in progress, Sterile alpha and armadillo motif-containing protein (SARM1) was reported to regulate terminal cell lysis following stimulation of the NLRP3 inflammasome [40], and like CARD19, also localizes to the mitochondrial outer membrane [33]. We therefore considered the possibility that SARM1 might contribute to cell lysis via interaction with CARD19. Unexpectedly however, BMDMs isolated from multiple independent lines of *Sarm1^-/-* mice (described further in Materials and Methods), including *Sarm1^-/-* mice reported by Carty *et al.* [40] and originally described by Kim et al [74], exhibited no defect in their ability to undergo cell lysis in response to canonical NLRP3 inflammasome stimuli (**S3A Fig**), nor did they exhibit elevated levels of inflammasome-dependent IL-1β release (**S3B Fig**). *Sarm1^-/-* BMDMs also showed wild-type levels of Caspase-1, GSDMD, and IL-1β processing (**S3C and S3D Fig**). Moreover, TNF release was unaffected in cells lacking SARM1 compared to WT controls, indicating that the NLRP3 inflammasome priming step (NF-κB pathway) is not dysregulated by the absence of SARM1 (**S3E Fig**). Furthermore, in contrast to *Card19^lxcn* BMDMs, the *Sarm1^-/-* macrophage lines had wild-type levels of cell death and cytokine release in response to non-canonical inflammasome activation (**S3F and S3G Fig**). Notably, some *Sarm1^-/-* lines were reported to contain a passenger mutation in the closely-linked gene *Xaf1*, indicating that some previous cell death-related phenotypes attributed to SARM1 may be due to alteration of *Xaf1* [75]. Altogether, these findings indicate that the phenotype of *Card19^lxcn* BMDMs is not related to potential interactions with SARM1.

Next, to test the sufficiency of CARD19 to induce cell death, we generated immortalized *Card19^+/+* and *Card19^lxcn* bone marrow hematopoietic progenitors using the ER-HOXB8 system [76], and transduced the progenitors with CARD19-expressing lentiviral constructs. Unexpectedly, *Card19^lxcn* iBMDMs transduced with CARD19 displayed comparable death to vector control-transduced iBMDMs, raising questions as to whether CARD19-deficiency was directly responsible for the observed defect in caspase-dependent death in *Card19^lxcn* BMDMs (**Fig 7A**).
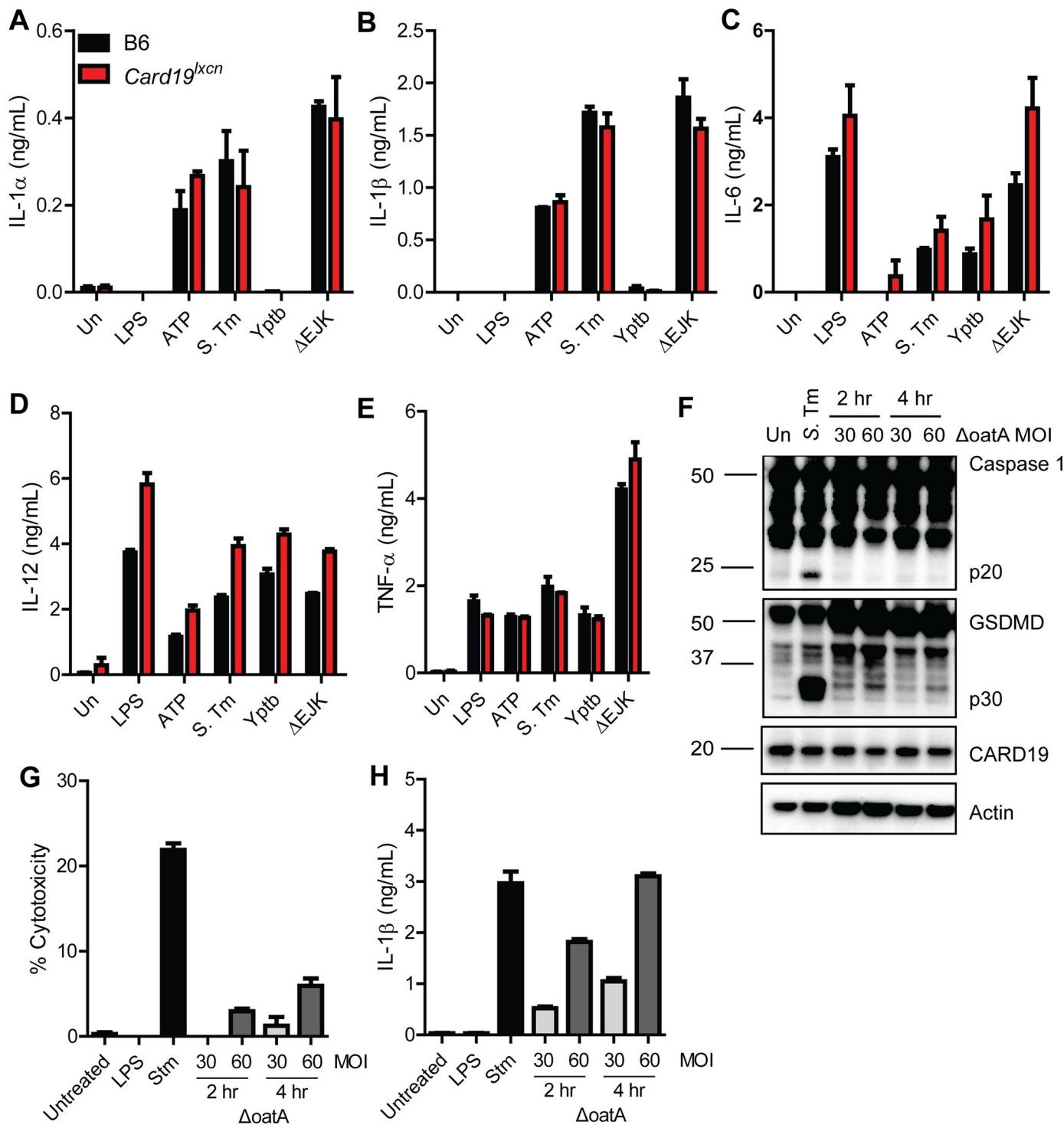
Fig 6. The cell death defect in *Card19*[lxcn] BMDMs is independent from cytokine release. (A-E) B6 (black bars) and *Card19*[lxcn] (red bars) BMDMs were primed with LPS for 3 hours and treated with extracellular ATP, infected with *S*. Tm, *Yptb*, or the *Yptb* ΔEJK strain lacking effectors YopE, YopJ and YopK. Supernatants were harvested 2 hours post-infection or ATP treatment and analyzed by ELISA for release of (A) IL-1α, (B) IL-1B, (C) IL-6, (D) IL-12, and (E) TNF-α. Mean ± SEM is displayed. Each figure is representative of 3 or more independent experiments. (F-H) B6 BMDMs were primed with LPS for 4 hours and infected with Δ*oatA S. aureus* or *S*. Tm. (F) Lysates were harvested at indicated times, run on SDS-PAGE page and analyzed by western blotting for Caspase 1, GSDMD, CARD19, or Actin (loading control). Supernatants were harvested at indicated time points and analyzed by (G) LDH for cytotoxicity and (H) ELISA for release of IL-1β. Each figure is representative of two independent experiments.

Passenger mutations in genes closely linked with the gene of interest in backcrossed C57BL/6 mice can confound interpretation of immune responses and cell death pathways in these lines [23,77,78]. Notably, *Card19^{lxcn}* mice were originally generated using 129SvEvBrd ESCs, and backcrossed for 10–12 generations [33]. *Card19^{+/lxcn}* and 129/SvIm/J BMDMs phenocopy wildtype BMDMs with respect to their ability to undergo terminal cell lysis in response to *S.* Tm., *Yptb*, and Sts, indicating that the phenotype is linked to the *Card19* locus (**S4A–S4C Fig**). To rule in or rule out the possibility that a passenger mutation linked to the *Card19* locus might be responsible, we next generated two independent *Card19*-deficient murine lines directly on the C57BL/6J background using CRIPSR/Cas9. The first of these removed exons 2–3, removing the entire CARD domain, but leaving a truncated mRNA that could produce a peptide fragment containing the transmembrane domain, which we termed *Card19^{ΔCARD}* (**S4D Fig** and **S1 Table**). The second was a complete deletion of the *Card19* locus, which we termed *Card19^{Null}* (see Materials and Methods for further details of construction of these lines). Critically, *Card19^{ΔCARD}* and *Card19^{Null}* BMDMs exhibited no observable defect in their ability to undergo cell lysis following infection with either *Yptb* or treatment with LPS+ATP, in contrast to BMDMs derived from the original *Card19^{lxcn}* line (**Fig 7B and 7C**). Altogether, these data indicate that loss of CARD19 is not the mechanistic basis of the defect in cell death seen in the original *Card19^{lxcn}* cells.

To identify the regions of the *Card19^{lxcn}* chromosome that may contain the original 129SvEvBrd lineage, we performed SNP genotyping analysis of the *Card19^{lxcn}* mice which indicated that approximately six megabases adjacent to the *Card19* locus were derived from the 129SvEvBrd lineage (**S5 Fig** and **S2 Table**). We additionally performed whole exome sequencing on B6 and *Card19^{lxcn}* mice to address the possibility that *Card19^{lxcn}* mice contain a functionally important polymorphism or have an expression defect in a gene closely linked to Card19. Although whole exome sequencing identified potential mutations in eight genes on chromosome 13, they were not high probability candidates (**S3 Table**).

We further performed RNA-seq on B6 and *Card19^{lxcn}* BMDMs, with the hypothesis that transcriptional alteration of genes closely linked to *Card19^{lxcn}* might result in the observed loss of cell lysis (**Fig 7D** and **S4 Table**). Intriguingly, *Ninj1*, recently identified as a key regulator of plasma membrane rupture during lytic cell death in response to apoptotic, pyroptotic and necrotic stimuli [41] is directly upstream of *Card19*, making it a likely candidate for passenger mutations or off-target effects (**S5 Fig, blue arrow**). *Card19^{lxcn}* and *Ninj1^{-/-}* BMDMs have a strikingly similar phenotype, as they both have a defect in cell lysis that is independent of IL-1 cytokine release and processing of caspases and gasdermins ([41], **Figs 1–6**). SNP mapping with a high-density SNP array identified a 129SvEvBrd-derived region in *Card19^{lxcn}* cells downstream of both *Ninj1* and *Card19* that also contained several B6 SNPs (**S2 Table** and **S5 Fig**). It is therefore likely that complex recombination occurred at the *Ninj1/Card19* locus. To test whether any mutations in *Ninj1* were present in the *Card19^{lxcn}* mice, we directly sequenced all 5 exons of *Ninj1*, including the 3' splice acceptor site for exon 2, reported to be mutated in the ENU-mutagenesis screen that first identified *Ninj1*, but were not able to detect any deviations from the reference genome in the *Ninj1* sequence in *Card19^{lxcn}* mice. However, *Ninj1* mRNA levels were reduced at baseline in *Card19^{lxcn}* BMDMs relative to wild-type BMDMs, and a knockout-validated antibody [41] demonstrated that NINJ1 protein levels were significantly reduced but not entirely absent in *Card19^{lxcn}* BMDMs (**Fig 7E**). Importantly, NINJ1 protein levels were not reduced in *Card19^{Null}* BMDMs (**Fig 7F**). To directly test whether loss of NINJ1 in the *Card19^{Lxcn}* BMDMs might be responsible for the defect in cell lysis, we reconstituted *Card19^{lxcn}* iBMDMs with *Ninj1* and electroporated with LPS. Critically, *Ninj1* reconstitution restored cell lysis to wildtype levels, similarly to the observations for *Ninj1^{-/-}* cells (**Figs 7G** and **S4B**). Altogether, our findings indicate that in addition to loss of
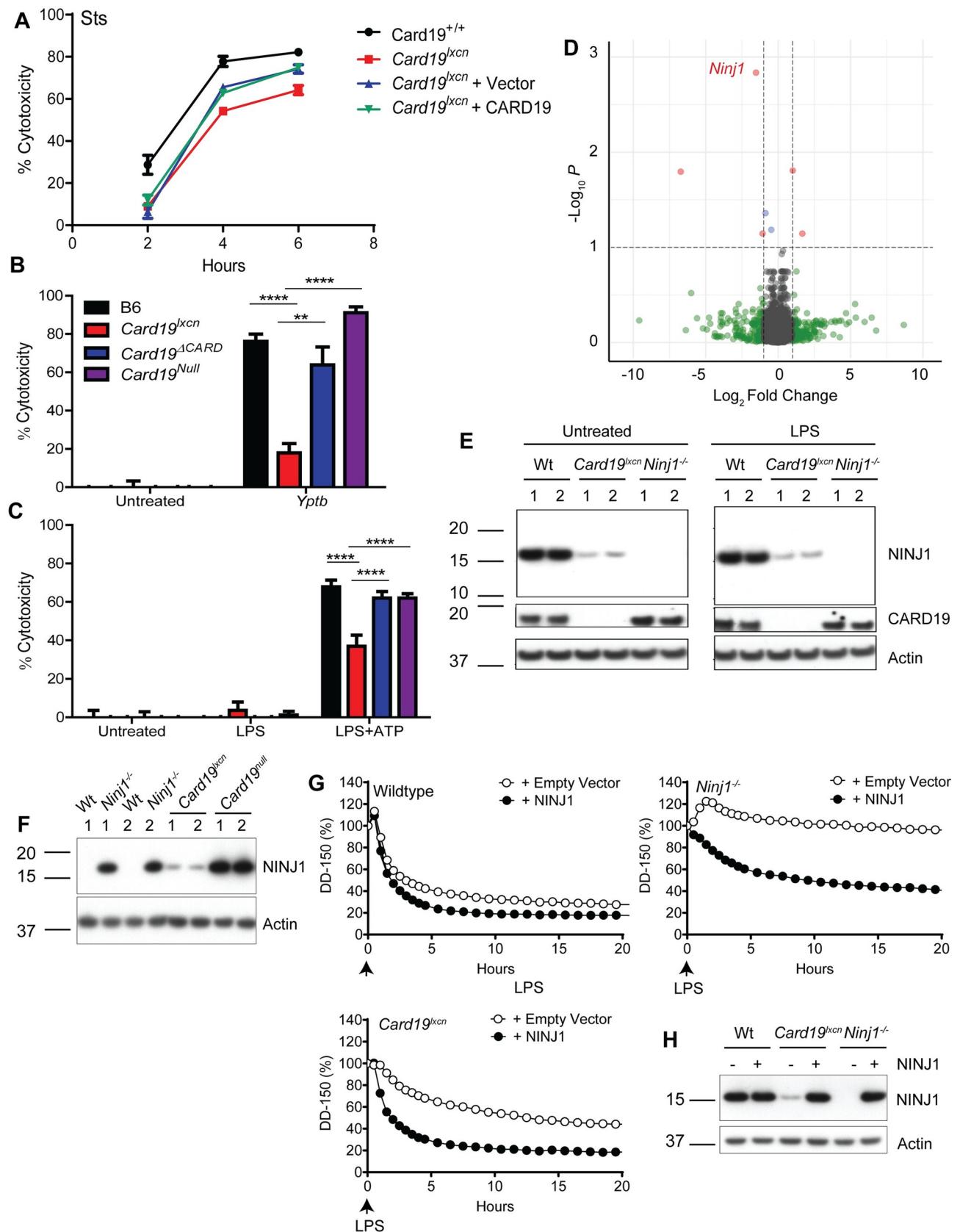
Fig 7. *Card19*^lxcn^ BMDMs are hypomorphic for *Ninj1* and reconstitution with *Ninj1* restores cell death. (A) *Card19*^lxcn^ immortalized murine progenitors were stably transduced with CARD19 or empty vector. Mature macrophages derived from untransduced immortalized progenitors *Card19*^lxcn^ and Card19^+/+^ and transduced immortalized progenitors *Card19*^lxcn^ + Vector and *Card19*^lxcn^ + CARD19 were treated with sts. Cell death was assayed by LDH release at indicated time points. Representative of three independent experiments. (B,C) B6, *Card19*^lxcn^, *Card19*^ΔCARD^, and *Card19*^Null^ BMDMs were treated with (B) *Yptb* or (C) LPS+ATP. Cell death was assayed by LDH release. Representative of three independent experiments. 2-way ANOVA with Bonferroni multiple comparisons post-test. **** p < 0.0001 *** p < 0.001 ** p < 0.01, * p < 0.05, n.s. not significant. (D) Volcano plot from RNA-seq analysis on untreated B6 and *Card19*^lxcn^ BMDMs showing differentially regulated genes. Genes whose expression is significantly altered are in red. *Ninj1* is marked. (E) BMDMs from B6, *Card19*^lxcn^, and *Ninj1*^-/-^ mice were primed with LPS or left untreated. Cell lysates were harvested, run on SDS-PAGE and analyzed by western blotting for CARD19, NINJ1, and Actin (cell lysate loading control). (F) BMDMs from B6, *Card19*^lxcn^, *Ninj1*^-/-^, and *Card19*^Null^ mice were left untreated. Cell lysates were harvested, run on SDS-PAGE and analyzed by western blotting for NINJ1, and Actin (cell lysate loading control). (G, H) Wildtype, *Ninj1*^-/-^ and *Card19*^lxcn^ iBMDMs were reconstituted with NINJ1 or empty vector. (G) Release of dextran dye-150 (DD-150) in live cell imaging analysis following LPS electroporation over a 20 hour time course. (H) Lysates of reconstituted cells were run on SDS-PAGE and analyzed by western blotting for NINJ1 and actin (cell lysate loading control). (E-H) Representative of two independent experiments.

CARD19, *Card19*^lxcn^ mice also have substantially reduced NINJ1 protein levels, most likely as a result of *Card19* targeting, leading to a defect in cell lysis consistent with the loss of NINJ1 function.

Card19^lxcn^ mice exhibit increased susceptibility to *Yersinia*

To assess whether the impact on cell death was biologically relevant during an *in vivo* infection in which cell death is important for systemic bacterial control, we infected *Card19*^lxcn^ mice with the gram-negative *Yersinia pseudotuberculosis* (*Yptb*). Consistent with findings that mice lacking essential mediators of cell death are more susceptible to bacterial infection [49,79–81], *Card19*^lxcn^ mice were significantly more susceptible to oral *Yptb* infection and had a defect in controlling systemic *Yptb* tissue burdens (**Fig 8A and 8B**). Interestingly, *Card19*^lxcn^ mice were equally susceptible to oral infection with *S.* Typhimurium (*S.* Tm), suggesting that cytokines released during GSDMD pore formation independent of cell lysis are sufficient to mediate control of *S.* Tm *in vivo* (**S6A Fig**). Importantly, *Card19*^Null^ mice did not have increased susceptibility to *Yptb*, indicating that loss of NINJ1 and not CARD19 is responsible for the phenotype of *Card19*^lxcn^ mice (**S6B Fig**). *Yptb*-infected *Card19*^lxcn^ mice exhibited increased splenomegaly (**Fig 8C and 8D**), suggesting either failure to control infection and elevated recruitment of inflammatory cells to the spleen, or a failure of innate cells to undergo cell death during bacterial infection *in vivo*. *Card19*^lxcn^ mice had similar levels of serum IL-6 and IL-12, although they had increased levels of TNF, consistent with their increased bacterial burden (**Fig 8E**). *Yptb*-induced cell death is dependent on caspase-8 [49,80]. We therefore also infected *Ripk3*^-/-^*Casp8*^-/-^ mice with *Yptb* to determine whether the phenotype of mice deficient in cell lysis due to hypomorphic Ninj1 expression is similar to that of mice lacking caspase-8. Notably, and consistent with our prior studies on caspase-8, *Yptb* oral infection led to rapid acute lethality in *Ripk3*^-/-^*Casp8*^-/-^ mice (**S6C Fig**), suggesting that while NINJ1-dependent cell lysis contributes to host defense against *Yersinia*, additional caspase-8-dependent factors likely play a role as well. Altogether these data indicated that NINJ1-mediated cell lysis is not important for control of cell-intrinsic cytokine production but contributes to host defense against bacterial infection.

Discussion

Our study has revealed that *Card19*^lxcn^ BMDMs are resistant to cell lysis during both pyroptosis and caspase-8-mediated apoptosis while maintaining caspase activation and release of IL-1 family cytokines. This data highlights the existence of a regulatory checkpoint downstream of gasdermin processing that controls the cell fate choice to undergo terminal cell lysis. Until recently, caspase-dependent cleavage of gasdermin D, and the subsequent release of the
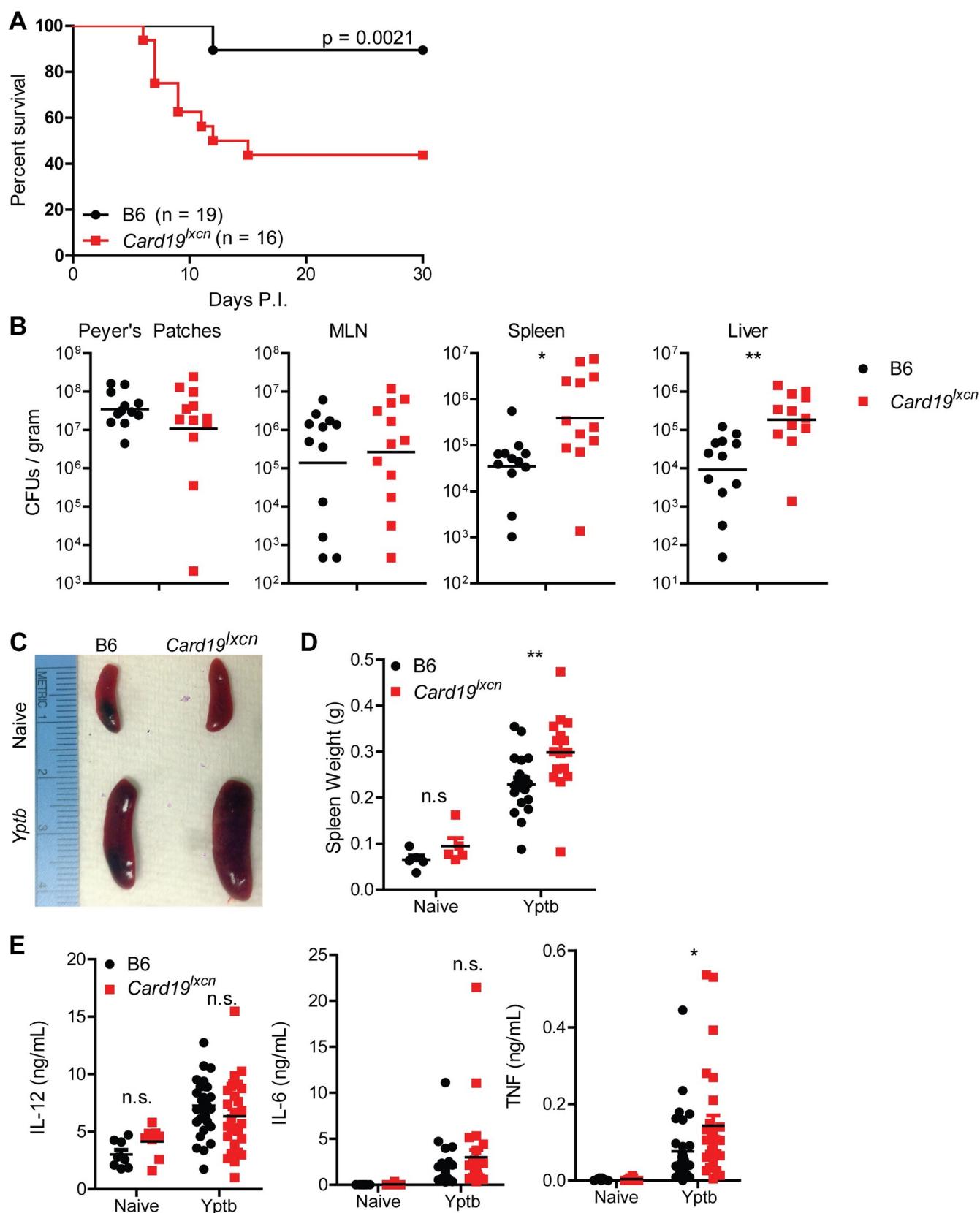
Fig 8. NINJ1 mediates anti-*Yersinia* host defense. (A) Survival of B6 and *Card19*[lxcn] mice following oral infection 10^8 CFUs of strain IP2777 *Yptb*. Data are pooled from two independent experiments that each gave similar results. Log-rank (Mantel-Cox) Survival test. (B) Bacterial CFUs per gram tissue in Peyer's Patches, MLN, Spleen and Liver in B6 and *Card19*[lxcn] mice seven days post-oral infection with *Yptb*. Representative of two (PP) or four (MLN, Spleen, Liver) independent experiments. Unpaired Student's *t*-test. ** p < 0.01, * p < 0.05. (C) Representative images of naive and *Yptb*-infected B6 and *Card19*[lxcn] spleens, seven days post-infection Representative of three independent experiments. (D) Quantification of naive and infected spleen weights. Data are pooled from three independent experiments. Naive (n = 5), *Yptb* (B6 n = 19, *Card19*[lxcn] n = 16) 2-way ANOVA with Bonferroni multiple comparisons post-test. ** p < 0.01. (E) Serum cytokines from naive and *Yptb* infected B6 and *Card19*[lxcn] mice. Data are pooled from four independent experiments. Naïve (n = 8), *Yptb* (B6 n = 31, *Card19*[lxcn] n = 28) 2-way ANOVA with Bonferroni multiple comparisons post-test. * p < 0.05, n.s. not significant.

gasdermin D N-terminal pore-forming domain was viewed as the terminal step in lytic cell death. However, some cell types or stimuli trigger IL-1β release without cell lysis, indicating that these are distinct cellular responses that can be decoupled [28,29,31,82]. Moreover, the recent observation that GSDMD-dependent release of IL-1β is regulated by charge-charge interactions highlights the selective nature of the GSDMD pore. That gasdermin-dependent secretion of IL-1 cytokines can be uncoupled from cell lysis further points to regulatory steps subsequent to cleavage and activation of gasdermin D that can be engaged to promote or limit cell lysis.

While our initial observations that *Card19*[lxcn] macrophages were resistant to cell lysis despite having wild-type levels of GSDMD processing suggested that CARD19 might regulate cell lysis, two CRISPR/Cas9-generated lines of mice that we generated directly on a B6 background (*Card19*[ΔCARD] and *Card19*[Null]) did not recapitulate this phenotype. Moreover, expressing CARD19 in *Card19*[lxcn] cells did not complement the lysis phenotype. These findings indicated that a CARD19-independent factor that was presumably affected in *Card19*[lxcn] mice was most likely responsible for the resistance of *Card19*[lxcn] cells to cell lysis. Intriguingly, *Ninj1* which is immediately upstream of *Card19* on chromosome 13, regulates cell lysis in response to pyroptotic and apoptotic stimuli [41]. *Ninj1* encodes a protein whose function was previously linked to axonal guidance, and was identified in a forward genetic screen for regulators of cell death [41]. The phenotype of *Ninj1*^{-/-} cells is strikingly similar to that of *Card19*[lxcn] BMDMs [41]. Although we were unable to identify any mutations in the NINJ1 coding sequence or intronic splice acceptor that would indicate a potential defect in NINJ1 in *Card19*[lxcn] mice, *Card19*[lxcn] BMDMs have substantially diminished levels of NINJ1 gene and protein expression, implicating NINJ1 as the likely driver for the phenotype in the *Card19*[lxcn] line. Furthermore, reconstitution of *Ninj1* in *Card19*[lxcn] iBMDMs restored wildtype levels of cell lysis following LPS electroporation. Together, these results indicate that genetic targeting of *Card19* resulted in an off-target effect on NINJ1 expression, leading to impaired terminal cell lysis and anti-*Yersinia* defense.

Unintended off-target effects on neighboring genes following genetic targeting have previously been reported. Notably, insertion of a PGK-Neo cassette into the granzyme B locus and β-globin locus control regions was found to disrupt multiple genes in the surrounding area [83]. Targeting of exons 13–16 of SH3 and multiple ankyrin repeat domains 3 (Shank3B) with a neomycin resistance cassette resulted in altered expression of neighboring genes as well as increased expression of exons 1–12 and the formation of an unusual Shank3 isoform not expressed in wildtype mice [84]. Furthermore, RNA-seq analysis of target and neighboring gene expression in a number of homozygous mutants revealed increased frequency of downregulated neighboring genes that would be expected due to local transcription dysregulation [85]. Our finding that genetic targeting of *Card19* resulted in decreased expression of *Ninj1* are consisted with these reports. Our findings underscore the complexity of genetic manipulation in mice and the importance of complementation analyses in validating knockout phenotypes.

In addition to the finding that NINJ1 regulates cell lysis, two separate CRISPR-based screens revealed the Ragulator/Rag/mTORC pathway as being important for GSDMD-dependent pore formation as well as *Yersinia*-induced activation of caspase-8, although they propose distinct roles for the function of the Ragulator complex in cell death [86,87]. Intriguingly, Evavold *et al*. propose that the Ragulator complex acts downstream of GSDMD cleavage to mediate pore formation, but upstream of NINJ1-induced cell lysis, whereas NINJ1 acts subsequent to pore formation to induce membrane rupture and ultimate cytolysis. Thus, in contrast to initial models proposing that release of the N-terminal portion of GSDMD was necessary and sufficient to trigger cell lysis, these findings collectively support a multi-step regulated process, downstream of GSDMD cleavage, that ultimately triggers lytic rupture of the cell.

How terminal cell lysis occurs downstream of GSDMD cleavage or plasma membrane insertion remains enigmatic. The mitochondrial protein SARM1 was previously reported to regulate cell lysis in response to NLRP3 inflammasome activation independently of IL-1β cytokine release. Mitochondrial disruption is a feature of both lytic and apoptotic forms of cell death, and the N-terminal GSDMD fragment is recruited to the mitochondrial membrane as well [73,88]. Unexpectedly however, primary macrophages generated from four independent lines of *Sarm1*$^{-/-}$ BMDMs had wild-type levels of cell lysis and IL-1β cytokine release. Whether passenger mutations, which have been reported in *Sarm1*$^{-/-}$ murine lines [75], may account for the reported phenotype of *Sarm1*$^{-/-}$ BMDMs, remains to be determined. Precisely how cell lysis can be uncoupled from IL-1 cytokine release remains a key unanswered question in this field. BMDMs from *Card19*^{lxcn}, *Ninj1*$^{-/-}$, and *Rag*$^{-/-}$ mice all display reduced cell lysis despite substantial levels of IL-1β cytokine release, similar to the hyperactivation phenotype previously described by Kagan and colleagues [30,31]. However, we observed that BMDMs induced to undergo hyperactivation following infection with Δ*oatA* mutant *S. aureus* exhibit reduced levels of total caspase-1 and GSDMD cleavage, suggesting that the regulated step in hyperactivation occurs at the level of caspase processing or complex assembly, rather than at the level of GSDMD pore formation.

In addition to demonstrating that terminal cell lysis is a regulated step downstream of GSDMD activation, this study extends our understanding of the role of lytic cell death in antibacterial host defense. *Card19*^{lxcn} mice showed significantly increased susceptibility to *Yersinia* infection, with higher systemic burdens and reduced ability to survive infection, consistent with our previous studies demonstrating that the RIPK1-Casp8-dependent cell death pathway enables activation of cytokine production from uninfected bystander cells. Interestingly, *Ripk3*$^{-/-}$*Casp8*$^{-/-}$ mice were even more susceptible to *Yptb* infection, which could be due to the fact that caspase-8-deficient cells are completely resistant to *Yptb*-induced cell death, or that caspase-8 also has cell-death-independent functions in regulating inflammatory cytokine production [89–91]. Altogether, our work highlights cell lysis and the release of inflammatory mediators from ruptured cells as a component of inflammatory responses that play an important role in mediating anti-microbial immune defense.

Materials and methods

Ethics statement

All animal studies were performed in compliance with the federal regulations set forth in the Animal Welfare Act (AWA), the recommendations in the Guide for the Care and Use of Laboratory Animals of the National Institutes of Health, and the guidelines of the University of Pennsylvania Institutional Animal Use and Care Committee. All protocols used in this study were approved by the Institutional Animal Care and Use Committee at the University of Pennsylvania, (Animal Welfare Assurance Number D16-00045/A3079-01, Protocol #804523).

All reagents and resources are listed in S5 Table.

Generation of Card19$^{\Delta CARD}$ mice

Card19$^{\Delta CARD}$ mice were produced by the CRISPR/Cas9 Mouse Targeting Core (PSOM-U-Penn) using CRISPR/Cas9 technology (flanking sgRNA and Cas9mRA microinjected in 1-cell mouse embryos), and a targeting strategy resulting in removal of exons 2–3. The resulting CARD19 deletion removes amino acids 3–99 including the entire CARD and giving a predicted protein product of 87 AA in length.

CARD19 5' Target Sequence: GAGATACTGGTGGGACCGAAGGG.
CARD19 3' Target Sequence: TTGGTCACACTTCGCTGAGATGG.
Mice were backcrossed onto C57BL/6J for at least 2 consecutive generations.

Generation of *Card19^{Null}* mice

Card19^{Null} mice were produced by the CRISPR/Cas9 Mouse Targeting Core (PSOM-UPenn) using CRISPR/Cas9 technology (flanking sgRNA and Cas9mRA microinjected in 1-cell mouse embryos), and a targeting strategy resulting in deletion of exon 1, resulting in the premature appearance of a stop codon and degradation by nonsense-mediated decay.

CARD19 5' Target Sequence: TAGGCGAAGGGACGCCGACCCGG.
CARD19 3' Target Sequence: GTTTCTGGTACGAGCTGGCAGGG.
Mice were backcrossed onto C57BL/6J for at least 2 consecutive generations.

Differentiation of murine bone marrow-derived macrophages (BMDMs)

Bone marrow derived macrophages were isolated and differentiated as previously described [92]. Briefly, isolated bone marrow cells from 6–10 week old male and female mice were grown at 37˚C, 5% CO_2 in 30% macrophage media (30% L929 fibroblast supernatant, complete DMEM). BMDMs were harvested in cold PBS on day 7, and replated in 10% macrophage media onto tissue culture (TC)-treated plates and glass coverslips in TC-treated plates. *Sarm1(AGS3)$^{-/-}$*, *Sarm1(AGS12)$^{-/-}$*, and *Sarm1(AD)$^{-/-}$* were previously described and provided by Adolfo-Garcia Sastre (Icahn School of Medicine at Mount Sinai) along with wildtype controls [74,75,93].

Bacterial culture and infection conditions

Bacteria strains used include *Yersinia pseudotuberculosis* (*Yptb*) strain IP2666, *Yptb* ΔEJK (lacking Yop effector proteins YopE, YopJ, and YopK), *Salmonella enterica* serovar Typhimurium strain SL1344 (*S.* Tm), DH5α *E. coli*, and Δ*oatA Staphylococcus aureus*. Bacterial strains were grown as previously described [26,49,71]. Briefly, bacteria were grown with aeration and specific antibiotics at 28˚C (*Yersinia*, irgasan) or 37˚C (*Salmonella*, streptomycin, *E. coli*, none, *S. aureus*, kanamycin). *Yersinia* strains were induced prior to infection by diluting the overnight culture 1:40 in 3 mL of inducing media (2xYT broth, 20 mM Sodium Oxalate, 20 mM $MgCl_2$). Inducing culture were grown at 28˚C for 1 hour and shifted to 37˚C for two hours with aeration. *Salmonella* strains were induced prior to infection by diluting the overnight culture 1:40 in 3 mL inducing media (LB broth, 300 mM NaCl), and grown standing for 3 hours at 37˚C. Δ*oatA S. aureus* was grown overnight in Todd Hewitt Broth at 37˚C with aeration [26]. Bacterial growth was measured using OD_{600} on a spectrophotometer. Bacteria were pelleted, washed, and resuspended in DMEM or serum-free media for infection. *In vitro* infections were performed at MOI 10 (*Yptb* and *S.* Tm, fractionation and microscopy), MOI 20 (*Yptb*, *ΔEJK* and *S.* Tm, all other assays) or MOI 30 (*E. coli*, LDH) unless otherwise noted. Δ*oatA* infections were performed at MOI 30 and 60. Thioglycolate *in vitro* infections were

performed at MOI 10. Gentamycin (100 μg/mL) was added one hour post infection for all infections.

Mouse strains

Card19^{lxcn} mice were previously described [33] and maintained as a breeding line in-house. This strain has been deposited at the Jackson Laboratory and is available as B6.129-*Card19tm1Lex*/SchaJ, Stock No. 036463. B6 and *Casp1*/*Casp11^{-/-}* mice obtained from Jackson Laboratories and subsequently maintained as a breeding line in-house. Previously published knockout mouse lines that were used to generate BMDMs are indicated in S1 Table. *Gsdmd^{-/-}* BMDMs were previously described [94], provided by Russell Vance, and maintained as a breeding line in-house. *Ripk3^{-/-}* mice [95] were a gift of Kim Newton and Vishva Dixit (Genentech) and *Ripk3/Casp8^{-/-}* mice [96] were a gift of Doug Green (St. Jude Children's Hospital). *Casp11^{-/-}* mice were originally generated by Junying Yuan [97] (Harvard University) and kindly provided by Tiffany Horng (Harvard University). *Sarm1(MSD)^{-/-}* mice were a gift from Adriano Aguzzi (University Hospital Zurich). Breeders were routinely genotyped. Mice were maintained in a specific pathogen-free facility by University Laboratory Animal Resources (ULAR) staff in compliance with IACUC approved protocols.

Generation of immortalized *Card19^{lxcn}* myeloid progenitors using ER-HOXB8

Card19^{lxcn} murine myeloid progenitors were immortalized using the ER-HoxB8 system [76]. Bone marrow was harvested from female mice and myeloid progenitors were isolated using a Percoll density gradient. Progenitors were plated in 5% SCF-conditioned media supplemented with 10 ng/mL IL-3 and IL-6 for three days. Progenitors were spinfected on fibronectin coated plates with ER-HoxB8 retrovirus in 25 ug/mL polybrene at 1000g for 90 minutes. Progenitors were supplemented with 0.5 uM estrogen and 10 ng/mL GM-CSF to induce macrophage progenitor differentiation. Progenitors were replated with fresh estrogen and GM-CSF for two days. Retrovirally infected cells were selected for with the addition of 1 mg/mL geneticin for 2–3 days. Progenitors were harvested and passaged until immortalization was confirmed by the death of all uninfected control cells. Mature macrophages were generated from immortalized progenitors by plating cells in 30% macrophage media and growing for 5–6 days. Cells were fed with additional macrophage media on day 3.

Transduction of *Card19^{lxcn}* immortalized progenitors

HEK293T cells were transfected using Lipofectamine 2000 with pCL-Eco retroviral packaging vector and MSCV2.2-CARD19 or empty vector (MSCV2.2). Successful transfection was confirmed by imaging under a widefield as MSCV contains IRES-GFP. *Card19^{lxcn}* ER-HoxB8 immortalized progenitors were spinfected with filtered viral supernatants from transfected HEK293T cells at 2500 RPM for 90 minutes. Transduced progenitors were transduced a second time the following day as before to increase infection efficiency. Progenitors were allowed to recover and proliferate prior to 2.5 ug/mL puromycin selection. A 95%+ pure population was isolated by flow cytometry sorting on GFP+. Mature macrophages were generated from immortalized, transduced progenitors by plating cells in 30% macrophage media and growing for 5–6 days, with additional media supplementation on day 3.

NINJ1 reconstitution

Wildtype, *Ninj1^{-/-}* and *Card19^{lxcn}* iBMDMs were reconstituted with Ninj1 as previously described [41]. Briefly, iBMDMs were co-electroporated with NINJ1/the piggyBac vector

BH1.11 and the transposase vector pBo using Neon electroporator. 6.25 ug/mL blasticidin was used for selection.

Plasmids and constructs

All constructs are listed in S5 Table. pcDNA3.1/CARD19-FLAG was obtained from GenScript (Refseq NM_026738.2). CARD19 was amplified and inserted into MSCV2.2 using Gibson cloning. All constructs were confirmed by sequencing prior to experimentation.

Cell death assays–LDH, PI uptake, & Dextran Dye-150 release

LDH. Triplicate wells of BMDMs were seeded in TC-treated 96 well plates. BMDMs were infected with indicated bacterial strains as indicated above. BMDMs were primed with 100 ng/mL LPS for 3 hours followed by 2.5 mM ATP treatment. BMDMs were treated with 10 uM staurosporine or 100 uM etoposide. BMDMs were pretreated with 100 uM zVAD(OMe)-FMK or 100 ug/mL cycloheximide for 1 hour before treatment with 100 ng/mL LPS. For non-canonical inflammasome cell death, BMDMs were primed with 400 ng/mL Pam3CSK4 for 3 hours and then infected with DH5α *E. coli*, MOI 30 for 16–20 hours. 100 ug/mL gentamycin was added one hour post treatment to all infectious experimental conditions. BMDMs were primed with LPS (100 ng/ml) for 4 hours and stimulated with nigericin (5 μM). BMDMs were primed with Pam3CSK4 (1 μg/ml) for 4 h and were transfected with 2 μg/ml E. coli O111:B4 LPS with Fugene HD. At indicated time points, plates were spun down at 250g and supernatants were harvested. Sups were combined with LDH substrate and buffer according to the manufacturer's instructions and incubated in the dark for 35 min. Plates were read on a spectrophotometer at 490 nm. Percent cytotoxicity was calculated by normalizing to maximal cell death (1% triton) and no cell death (untreated cells).

PI uptake. Propidium Iodide uptake was performed as previously described [26]. Briefly, triplicate wells of BMDMs were seeded in TC-treated black-walled 96 well plates. BMDMs were infected or treated as described above in 50 uL HBSS plus 10% FBS. Propidium Iodide (2x, 10 uM) was added in 50 uL HBSS to each well and incubated for 5 minutes in the dark to allow for stabilization of the signal in the maximal cell death wells (1% triton). PI uptake was detected by fluorescence on a BioTek Synergy HT Multi-Detection Microplate Reader (540/25 excitation, 590/35 emission, sensitivity 35, integration time 1 sec) every 2.5 minutes (*S*. Tm., ATP) or every 10 minutes (*Yptb*, Sts) for the indicated time points. Gentamycin (100 ug/mL) was added one hour post infection (*Yptb*, Sts). Percent cytotoxicity was calculated as described above.

Dextran Dye-150 (DD-150) release. DD-150 release was performed as previously described [41]. Briefly, 5.0×10^6 BMDMs were loaded with DD-150 (50 mg/mL) via electroporation in R buffer. Prior to plating, BMDMs were washed with high-glucose DMEM. Following stimulation, images of BMDMs were scanned over 20 h with IncuCyte S3 (Essen BioScience) at 10X magnification.

Confocal microscopy

BMDMs were seeded as described above, treated with staurosporine for indicated time points, fixed, permeabilized, and blocked. BMDMs were stained for HMGB1 (1:200) at 37°C for 1 hr, Alexa Fluor rabbit 488 (1:4000) at RT for 1 hr, and Hoechst and Phalloidin at RT for 30 min. Slides were imaged as described above, with a single z-plane taken per field. Percent nuclear HMGB1 was quantified by identifying total HMGB1 staining per cell and comparing the overlap with nuclear staining (Hoechst). 65–200 cells were analyzed per genotype and condition. Cloud analysis was completed by counting the number of HMGB1 clouds per field of view with 5–8 fields per condition.

Caspase 8 activity

BMDMs were seeded as described above in a white-walled 96 well plate and treated with *Yptb* or Sts for the indicated times. Z-IETD-fmk (500 uM, SM Biochemicals) was added 1 hour prior to infection/treatment as a control to block caspase-8 activity. Caspase-8 activity was detected using Caspase-8 Glo (Promega) according to the manufacturer's instructions. Luminescence was read on a Gen5 plate reader.

Western blots

BMDMs were seeded in TC-treated 24 or 12 well plates. Necrostatin (60 uM, Nec-1) was used to inhibit RIPK1 activity for 1 hour prior to *Yptb* infection. Following infection or treatment in serum-free media, supernatants were harvested and TCA precipitated. Briefly, supernatants were spun down to remove cell debris and TCA precipitated overnight at 4˚C. Sups were spun down and washed with acetone. Remaining TCA was neutralized with Tris, and the pellet was resuspended in 5x sample buffer (125 mM Tris, 10% SDS, 50% glycerol, 0.06% bromophenol blue, 1% β-mercaptoethanol). BMDMs were lysed in lysis buffer (20 mM HEPES, 150 mM NaCl, 10% glycerol, 1% Triton X-100, 1mM EDTA, pH7.5) plus 1x complete protease inhibitor cocktail and 1x sample buffer (25 mM Tris, 2% SDS, 10% glycerol, 0.012% bromophenol blue, 0.2% β-mercaptoethanol). Lysates and supernatants were boiled and centrifuged at full speed for 5 minutes, and sups were run on 4–12% polyacrylamide gels and transferred to PVDF. Membranes were immunoblotted using the following primary antibodies: β-Actin (1:5000), Bid (1:500), CARD19 (1:500), Caspase 1 (1:360), Caspase 3 (1:1000), Caspase 8 (1:1000), GSDMD (1:1000), HMGB1 (1:1000), GSDME (1:500), PARP (1:1000), NINJ1, Tubulin, and IL-1β. Species specific HRP-conjugated secondary antibodies were used for each antibody (1:5000). Membranes were developed using Pierce ECL Plus and SuperSignal West Femto Maximum Sensitivity Substrate according to the manufacturer's instructions. Western blot time-courses were performed in parallel with cytotoxicity assays to accurately interpret protein release before and after overt cell death.

Cytokine release

Triplicate wells of BMDMs were seeded in TC-treated 48 well plates. All conditions except untreated were primed with 100 ng/mL LPS for 3 hrs or unless otherwise indicated. BMDMs were infected with bacterial strains or treated with 2.5 mM ATP. BMDMs were primed with LPS (100 ng/ml) for 4 hours and stimulated with nigericin (5 μM). IL-1β release were measured at the indicated time points. BMDMs were primed with LPS (100 ng/ml) and TNF release was measured after 4 hours. BMDMs were primed with Pam3CSK4 (1 μg/ml) for 4 h and were transfected with 2 μg/ml E. coli O111:B4 LPS with Fugene HD. IL-1β release were measured after 16 h. ELISA supernatants were added to IL-1α, IL-1β, IL-6, IL-12, and TNF-α capture antibody-coated 96-well plates and incubated at 4˚C overnight. Plates were incubated with the appropriate biotinylated antibodies in 1% BSA, followed by streptavidin. ELISA was developed with o-phenylenediamine dihydrochloride in citric acid buffer and stopped with 3M sulfuric acid. Plates were read on a spectrophotometer at 490 nm.

Hyperactivation

Triplicate wells of BMDMs were seeded in TC-treated 48 well plates (ELISA, LDH), and 12 well plates (western). All conditions except untreated were primed with 1 ug/mL LPS for 4 hrs. BMDMs were infected with *S.* Tm. (MOI 20) or *ΔoatA S. aureus* (MOI 30 or 60) as described above. Gentamycin (100 ug/mL) was added 1 hr post infection. Sups and lysates were

harvested at 30 min (*S.* Tm.) or 2 and 6 hrs (*ΔoatA*) and analyzed by ELISA for IL-1B release, by LDH for cytotoxicity, or by western blotting for caspase-1, GSDMD, CARD19, and actin (loading control).

SNP sequencing

Tails from four *Card19*[lxcn] mice were sent to Dartmouse for a genetic background check. Each sample was interrogated over 5300 SNPs space along the mouse genome with an average density of 0.5 Mbp using an Illumina Infinium Genotyping Assay.

Whole exome sequencing

Genomic DNA was extracted from 1 B6 and two *Card19*[lxcn] BMDMs derived from three independent mice using a DNeasy blood and tissue kit (Qiagen) according to the manufacturer's instructions. gDNA was shipped to Genewiz for Illumina HiSeq 2x150 bp sequencing. C57BL/6J was used as a reference genome.

RNA-seq

B6 and *Card19*[lxcn] BMDMs were prepared as above from 3 independent mice per genotype. 1×10^6 BMDMs were treated with 100 ng/mL LPS for 3 hours or left untreated. RNA was extracted using the RNeasy Plus Mini Kit (Qiagen) according to the manufacturer's instructions. Sequence-ready libraries were prepared using the Illumina TruSeq Total Transcriptome kit with Ribo-Zero Gold rRNA depletion (Illumina). Quality assessment and quantification of RNA preparations and libraries were carried out using an Agilent 4200 TapeStation and Qubit 3, respectively. Samples were sequenced on an Illumina NextSeq 500 to produce 75–base pair single end reads with a mean sequencing depth of 35 million reads per sample. Raw reads from this study were mapped to the mouse reference transcriptome (Ensembl; Mus musculus GRCm38) using Kallisto version 0.46.2 [98]. Raw sequence data are available on the Gene Expression Omnibus (GEO; accession no. GSE168489)

All subsequent analyses were carried out using the statistical computing environment R version 4.0.3 in RStudio version 1.2.5042 and Bioconductor [99]. Briefly, transcript quantification data were summarized to genes using the tximport package [100] and normalized using the trimmed mean of M values (TMM) method in edgeR [101]. Genes with <1 CPM in 2 samples were filtered out. Normalized filtered data were variance-stabilized using the voom function in limma [102], and differentially expressed genes were identified with linear modeling using limma (FDR $\leq$ 0.10; absolute $\log_2$FC $\geq$ 1) after correcting for multiple testing using Benjamini-Hochberg. Volcano plots were made using the Enhanced Volcano package [103].

Mouse infections

Age and sex-matched B6, *Card19*[lxcn], *Card19*[Null], *Ripk3*^{-/-}, and *Ripk3*^{-/-}*Casp8*^{-/-} mice between 8–12 weeks were orally infected with 10^8 CFU of *Yersinia pseudotuberculosis* strain IP2777 after fasting overnight. Mice were monitored for survival for 30 days or were euthanized using CO_2 followed by cervical dislocation, in compliance with IACUC approved euthanasia protocols. Blood was harvested by cardiac puncture following death. Serum cytokine levels (IL-6, IL-12, TNF-α) were measured by ELISAs as described above. Spleen, liver, mesenteric lymph nodes, and Peyer's patches were removed, weighed, homogenized, diluted in PBS, and plated on LB agar plates with irgasan for CFUs. B6 and *Card19*[lxcn] were orally infected with 10^7 CFUs of *Salmonella enterica* serovar Typhimurium strain SL1344 after fasting overnight. Mice were monitored for survival for 30 days.

Thioglycolate injections

Age and sex-matched B6 and *Card19^lxcn^* mice between 9–11 weeks were injected intraperito-neally with 4% aged thioglycolate or PBS. 48 hours after injection, mice were euthanized using CO_2. The peritoneum was lavaged with 10 mL cold PBS and the peritoneal exudate cells were spun down. RBCs were lysed using RBC lysis buffer. PECS were counted using trypan blue exclusion on a hemocytometer and plated in complete DMEM without antibiotics in 96 well plates (1×10^5 cells for PBS PECS, 0.7×10^5 cells for TG PECS). Cells were washed with warm PBS to remove non-adherent cells and infected with *Yptb*, *S.* Tm. or treated with staurosporine as described above.

Statistical analysis

Statistical analysis was completed using GraphPad Prism. Two-tailed Student's *t* test or paired Student's *t* test were used for comparisons of two groups. One-way analysis of variance (ANOVA) with pairwise comparisons and Bonferroni post-test correction was used for multi-ple group comparisons. Repeated-measures ANOVA or paired *t* tests were used for matched samples. Studies were conducted without blinding or randomization. Values of $p < 0.05$ were considered statistically significant.

Supporting information

S1 Fig. CARD19 is required for optimal caspase-dependent cell death. Primary C57BL/6J (B6), *Card19^-/-^*, *Card19^+/+^*, and *Casp11^-/-^* BMDMs were treated with (A) *S.* Tm (B) *Yptb*, and cell death was assayed by LDH release. BMDMs were treated, supernatants were harvested from triplicate wells at indicated time points and measured for cytotoxicity. The mean ± SEM of means from triplicate wells from 3–19 independent experiments as indicated in parenthesis. *** $p < 0.001$, ** $p < 0.01$, * $p < 0.05$. n.s. not significant. 2-way ANOVA with Bonferroni mul-tiple comparisons post-test.
(TIF)

S2 Fig. *Card^lxcn^* BMDMs are not deficient for Caspase-1, or Caspase-8 activity. (A) B6, *Card19^lxcn^*, and *Gsdmd^-/-^* BMDMS were infected with *Yptb*. Cell death was assayed by LDH release. Representative of three independent experiments. (B-D) B6, *Casp1/11^-/-^*, *Ripk3^-/-^*, or *Ripk3^-/-^/Casp8^-/-^* BMDMs were left uninfected (Un) (B) infected with *Yptb*, (C) treated with sts or (D) infected with *S.* Tm in the presence of DMSO, the caspase-3/7 inhibitor DEVD, and the caspase-8 inhibitor IETD. Lysates were harvested (B, C) 3 hours or (D) 0.5 and 1 hour post treatment and analyzed by western blotting for GSDMD, DFNA5/GSDME, Caspase-1, and actin (loading control). Blots representative of two or three independent experiments.
(TIF)

S3 Fig. SARM1 does not regulate canonical and non-canonical inflammasome death and cytokine release. (A-D) *Sarm1(MSD)^-/-^*, *Sarm1(MSD)^+/-^*, *Sarm1(MSD)^+/+^*, C57BL/6, *Sarm1 (AGS3)^-/-^*, *Sarm1(AGS12)^-/-^* and *Sarm1(AD)^-/-^* BMDMs were primed with LPS (100 ng/ml) for 4 hours and stimulated with nigericin (5 μM). (A) LDH and (B) IL-1β release were measured at the indicated time points. (C) Supernatant and cell extract or (D) mixed supernatant and cell extract were examined by immunoblotting at the indicated time points. (E) BMDMs were primed with LPS (100 ng/ml) and TNF release was measured after 4 hours. (F and G) BMDMs were primed with Pam3CSK4 (1 μg/ml) for 4 h and were transfected with 2 μg/ml E. coli O111:B4 LPS with Fugene HD. (F) LDH and (G) IL-1β release were measured after 16 h. (A and B, E-G) Data are mean + SD of triplicate cell stimulation and is representative of two to four independent experiments. Immunoblots are representative of two independent

experiments.
(TIF)

S4 Fig. The defect in cell death is linked to the *Card19* locus. (A-C) B6, Card19^{lxcn}, Card19$^{+/lxcn}$, and 129/Sv BMDMs were treated with (A) *S*.Tm, (B) *Yptb* or (C) sts. Cell death was assayed by LDH release at indicated time points. Representative of three independent experiments. (D) CARD19 exon schematic showing each independent CARD19 mouse line with the respective CARD19 product.
(TIF)

S5 Fig. A six megabase region at the *Card19* locus remains homozygous for 129SvEvBrd.
(A) Chromosome 13 with tested SNPs from DartMouse genetic background check. C57BL/6 SNPs are in green, 129SvEvBrd SNPs are in yellow, and uninformative SNPs (i.e. not all samples gave identical results) are in black. The 10 megabase region on either side of the *Card19* locus is zoomed in below it with chromosomal locations noted in bold numbers and black notches. Genes in red are expressed in macrophages. *Ninj1* is in blue. The six megabase region highlighted by the yellow bar is homozygous for 129SvEvBrd. The green regions are homozygous for C57BL/6. A zoomed in region at *Card19* is highlighted with the original Lexicon Targeting strategy. (B) Wildtype, *Card19^{lxcn}, and Ninj1$^{-/-}$* iBMDMs were reconstituted with NINJ1/BH1.11 piggyBac or empty vector. Lysates were harvested and run on SDS-PAGE gel and probed for NINJ1 and actin (loading control).
(TIF)

S6 Fig. *Card19^{Null}* mice are not more susceptible to *Yersinia* than wildtype mice. (A) Survival of B6 and *Card19^{lxcn}* mice following oral infection 10^7 CFUs of strain SL1344 *S*. Tm. Data are from one experiment. (B) B6 and *Card19^{Null}* mice were orally infected with 10^8 CFUs of strain IP2777 *Yptb*. Seven days post infection, organs were harvested for enumeration. Data pooled from three independent experiments (B6 = 20, *Card19^{Null}* = 17). (C) Survival of B6, *Ripk3$^{-/-}$*, and *Ripk3$^{-/-}$Casp8$^{-/-}$* mice following oral infection 10^8 CFUs of strain IP2777 *Yptb*. Data are pooled from two independent experiments.
(TIF)

S1 Table. BMDM and Murine Sources. Sources of BMDMs and their derivation are listed in S1 Table.
(DOCX)

S2 Table. Chromosome 13 SNP Results. SNPs from DartMouse SNP genetic background check 10 megabases upstream and downstream of the *Ninj1/Card19* chromosome 13 locus. SNP identification and chromosomal position are indicated. SNPs are indicated as wildtype (B6) or 129SvEvBrd (129). The change, gene ID, gene name, and known function are listed. *Ninj1* and *Card19* are listed for reference.
(DOCX)

S3 Table. Chromosome 13 Whole Exome Sequencing Results. Chromosome 13 results are displayed from whole exome sequencing of *Card19^{lxcn}* mice.
(DOCX)

S4 Table. RNA-seq Results: Untreated B6 BMDMs vs. Untreated *Card19^{lxcn}* BMDMs. RNA-Seq results from untreated B6 and *Card19^{lxcn}* BMDMs.
(DOCX)

S5 Table. Key resources and reagents. Reagents and resources utilized are listed in S5 Table.
(DOCX)

Acknowledgments

Author Contributions

Conceptualization: Elisabet Bjanes, Igor E. Brodsky.

Formal analysis: Elisabet Bjanes, Rina Matsuda.

Funding acquisition: Jorge Henao-Mejia, Brian C. Schaefer, Igor E. Brodsky.

Investigation: Elisabet Bjanes, Reyna Garcia Sillas, Rina Matsuda, Benjamin Demarco, Timothée Fettrelet, Alexandra A. DeLaney, Opher S. Kornfeld, Bettina L. Lee, Eric M. Rodríguez López, Daniel Grubaugh, Meghan A. Wynosky-Dolfi, Naomi H. Philip, Elise Krespan, Dorothy Tovar.

Methodology: Elisabet Bjanes.

Resources: Elise Krespan, Leonel Joannas, Daniel P. Beiting, Jorge Henao-Mejia, Brian C. Schaefer, Petr Broz.

Supervision: Leonel Joannas, Jorge Henao-Mejia, Kaiwen W. Chen, Petr Broz, Igor E. Brodsky.

Writing – original draft: Elisabet Bjanes, Igor E. Brodsky.

Writing – review & editing: Elisabet Bjanes, Brian C. Schaefer, Kaiwen W. Chen, Igor E. Brodsky.

References

1. Mori C, Nakamura N, Kimura S, Irie H, Takigawa T, Shiota K. Programmed cell death in the interdigital tissue of the fetal mouse limb is apoptosis with DNA fragmentation. Anat Rec. 1995; 242(1):103–10. https://doi.org/10.1002/ar.1092420114 PMID: 7604973.

2. Rodriguez I, Ody C, Araki K, Garcia I, Vassalli P. An early and massive wave of germinal cell apoptosis is required for the development of functional spermatogenesis. EMBO J. 1997; 16(9):2262–70. https://doi.org/10.1093/emboj/16.9.2262 PMID: 9171341; PubMed Central PMCID: PMC1169828.

3. Kajstura J, Cheng W, Reiss K, Clark WA, Sonnenblick EH, Krajewski S, et al. Apoptotic and necrotic myocyte cell deaths are independent contributing variables of infarct size in rats. Lab Invest. 1996; 74 (1):86–107. PMID: 8569201.

4. Mariathasan S, Newton K, Monack DM, Vucic D, French DM, Lee WP, et al. Differential activation of the inflammasome by caspase-1 adaptors ASC and Ipaf. Nature. 2004; 430(6996):213–8. Epub 2004/06/11. https://doi.org/10.1038/nature02664 nature02664 [pii]. PMID: 15190255.

5. Miao EA, Alpuche-Aranda CM, Dors M, Clark AE, Bader MW, Miller SI, et al. Cytoplasmic flagellin activates caspase-1 and secretion of interleukin 1beta via Ipaf. Nat Immunol. 2006; 7(6):569–75. Epub 2006/05/02. ni1344 [pii]. https://doi.org/10.1038/ni1344 PMID: 16648853.

6. Monack DM, Mecsas J, Ghori N, Falkow S. Yersinia signals macrophages to undergo apoptosis and YopJ is necessary for this cell death. Proc Natl Acad Sci USA. 1997; 94(19):10385–90. https://doi.org/10.1073/pnas.94.19.10385 PMID: 9294220.

7. Zamboni DS, Kobayashi KS, Kohlsdorf T, Ogura Y, Long EM, Vance RE, et al. The Birc1e cytosolic pattern-recognition receptor contributes to the detection and control of Legionella pneumophila infection. Nat Immunol. 2006; 7(3):318–25. https://doi.org/10.1038/ni1305 PMID: 16444259.

8. Green DR, Ferguson T, Zitvogel L, Kroemer G. Immunogenic and tolerogenic cell death. Nat Rev Immunol. 2009; 9(5):353–63. Epub 2009/04/15. https://doi.org/10.1038/nri2545 PMID: 19365408; PubMed Central PMCID: PMC2818721.

9. Kerr JF, Wyllie AH, Currie AR. Apoptosis: a basic biological phenomenon with wide-ranging implications in tissue kinetics. Br J Cancer. 1972; 26(4):239–57. https://doi.org/10.1038/bjc.1972.33 PMID: 4561027; PubMed Central PMCID: PMC2008650.

10. Uchiyama R, Yonehara S, Taniguchi S, Ishido S, Ishii KJ, Tsutsui H. Inflammasome and Fas-Mediated IL-1beta Contributes to Th17/Th1 Cell Induction in Pathogenic Bacterial Infection In Vivo. J Immunol. 2017; 199(3):1122–30. https://doi.org/10.4049/jimmunol.1601373 PMID: 28674179.

11. Nagata S. Apoptosis and Clearance of Apoptotic Cells. Annu Rev Immunol. 2018. https://doi.org/10.1146/annurev-immunol-042617-053010 PMID: 29400998.

12. Samali A, Zhivotovsky B, Jones D, Nagata S, Orrenius S. Apoptosis: cell death defined by caspase activation. Cell Death Differ. 1999; 6(6):495–6. https://doi.org/10.1038/sj.cdd.4400520 PMID: 10381647.

13. Fink SL, Cookson BT. Apoptosis, pyroptosis, and necrosis: mechanistic description of dead and dying eukaryotic cells. Infect Immun. 2005; 73(4):1907–16. Epub 2005/03/24. 73/4/1907 [pii]. https://doi.org/10.1128/IAI.73.4.1907-1916.2005 PMID: 15784530.

14. Kayagaki N, Stowe IB, Lee BL, O'Rourke K, Anderson K, Warming S, et al. Caspase-11 cleaves gasdermin D for non-canonical inflammasome signalling. Nature. 2015; 526(7575):666–71. https://doi.org/10.1038/nature15541 Epub 2015 Sep 16. PMID: 26375259.

15. Martinon F, Burns K, Tschopp J. The inflammasome: a molecular platform triggering activation of inflammatory caspases and processing of proIL-beta. Mol Cell. 2002; 10(2):417–26. Epub 2002/08/23. S1097276502005993 [pii]. https://doi.org/10.1016/s1097-2765(02)00599-3 PMID: 12191486.

16. Shi J, Zhao Y, Wang K, Shi X, Wang Y, Huang H, et al. Cleavage of GSDMD by inflammatory caspases determines pyroptotic cell death. Nature. 2015; 526(7575):660–5. https://doi.org/10.1038/nature15514 PMID: 26375003.

17. Orning P, Weng D, Starheim K, Ratner D, Best Z, Lee B, et al. Pathogen blockade of TAK1 triggers caspase-8–dependent cleavage of gasdermin D and cell death. Science. 2018:eaau2818. https://doi.org/10.1126/science.aau2818 PMID: 30361383

18. Sarhan J, Liu BC, Muendlein HI, Li P, Nilson R, Tang AY, et al. Caspase-8 induces cleavage of gasdermin D to elicit pyroptosis during Yersinia infection. Proc Natl Acad Sci U S A. 2018; 115(46): E10888–E97. Epub 2018/11/02. https://doi.org/10.1073/pnas.1809548115 PMID: 30381458.

19. Chen KW, Demarco B, Heilig R, Shkarina K, Boettcher A, Farady CJ, et al. Extrinsic and intrinsic apoptosis activate pannexin-1 to drive NLRP3 inflammasome assembly. Embo j. 2019; 38(10). Epub 2019/03/25. https://doi.org/10.15252/embj.2019101638 PMID: 30902848; PubMed Central PMCID: PMC6517827.

20. Demarco B, Grayczyk JP, Bjanes E, Le Roy D, Tonnus W, Assenmacher CA, et al. Caspase-8-dependent gasdermin D cleavage promotes antimicrobial defense but confers susceptibility to TNF-induced lethality. Science advances. 2020; 6(47). Epub 2020/11/20. https://doi.org/10.1126/sciadv.abc3465 PMID: 33208362; PubMed Central PMCID: PMC7673803.

21. Demarco B, Chen KW, Broz P. Cross talk between intracellular pathogens and cell death. Immunological reviews. 2020; 297(1):174–93. Epub 2020/06/23. https://doi.org/10.1111/imr.12892 PMID: 32567717.

22. Cullen SP, Kearney CJ, Clancy DM, Martin SJ. Diverse Activators of the NLRP3 Inflammasome Promote IL-1beta Secretion by Triggering Necrosis. Cell Rep. 2015; 11(10):1535–48. https://doi.org/10.1016/j.celrep.2015.05.003 PMID: 26027935.

23. Kayagaki N, Warming S, Lamkanfi M, Vande Walle L, Louie S, Dong J, et al. Non-canonical inflammasome activation targets caspase-11. Nature. 2011; 479(7371):117–21. https://doi.org/10.1038/nature10558 PMID: 22002608.

24. Fink SL, Cookson BT. Caspase-1-dependent pore formation during pyroptosis leads to osmotic lysis of infected host macrophages. Cell Microbiol. 2006; 8(11):1812–25. https://doi.org/10.1111/j.1462-5822.2006.00751.x PMID: 16824040.

25. Verhoef PA, Kertesy SB, Lundberg K, Kahlenberg JM, Dubyak GR. Inhibitory effects of chloride on the activation of caspase-1, IL-1beta secretion, and cytolysis by the P2X7 receptor. J Immunol. 2005; 175 (11):7623–34. https://doi.org/10.4049/jimmunol.175.11.7623 PMID: 16301672.

26. Evavold CL, Ruan J, Tan Y, Xia S, Wu H, Kagan JC. The Pore-Forming Protein Gasdermin D Regulates Interleukin-1 Secretion from Living Macrophages. Immunity. 2018; 48(1):35–44 e6. https://doi.org/10.1016/j.immuni.2017.11.013 Epub 2017 Nov 28. PMID: 29195811; PubMed Central PMCID: PMC5773350.

27. Heilig R, Dilucca M, Boucher D, Chen KW, Hancz D, Demarco B, et al. Caspase-1 cleaves Bid to release mitochondrial SMAC and drive secondary necrosis in the absence of GSDMD. Life Science Alliance. 2020; 3(6):e202000735. https://doi.org/10.26508/lsa.202000735 PMID: 32345661

28. Gaidt MM, Ebert TS, Chauhan D, Schmidt T, Schmid-Burgk JL, Rapino F, et al. Human Monocytes Engage an Alternative Inflammasome Pathway. Immunity. 2016; 44(4):833–46. https://doi.org/10.1016/j.immuni.2016.01.012 Epub 2016 Mar 29. PMID: 27037191.

29. Chen KW, Gross CJ, Sotomayor FV, Stacey KJ, Tschopp J, Sweet MJ, et al. The neutrophil NLRC4 inflammasome selectively promotes IL-1beta maturation without pyroptosis during acute Salmonella challenge. Cell Rep. 2014; 8(2):570–82. https://doi.org/10.1016/j.celrep.2014.06.028 PMID: 25043180.

30. Zanoni I, Tan Y, Di Gioia M, Springstead JR, Kagan JC. By Capturing Inflammatory Lipids Released from Dying Cells, the Receptor CD14 Induces Inflammasome-Dependent Phagocyte Hyperactivation. Immunity. 2017; 47(4):697–709.e3. https://doi.org/10.1016/j.immuni.2017.09.010 PMID: 29045901.

31. Zanoni I, Tan Y, Di Gioia M, Broggi A, Ruan J, Shi J, et al. An endogenous caspase-11 ligand elicits interleukin-1 release from living dendritic cells. Science. 2016; 352(6290):1232–6. https://doi.org/10.1126/science.aaf3036 Epub 2016 Apr 21. PMID: 27103670; PubMed Central PMCID: PMC5111085.

32. Heilig R, Dick MS, Sborgi L, Meunier E, Hiller S, Broz P. The Gasdermin-D pore acts as a conduit for IL-1beta secretion in mice. Eur J Immunol. 2017. https://doi.org/10.1002/eji.201747404 PMID: 29274245.

33. Rios KE, Kashyap AK, Maynard SK, Washington M, Paul S, Schaefer BC. CARD19, the protein formerly known as BinCARD, is a mitochondrial protein that does not regulate Bcl10-dependent NF-κB activation after TCR engagement. Cellular Immunology. 2020; 356:104179. https://doi.org/10.1016/j.cellimm.2020.104179 PMID: 32763502

34. Woo HN, Hong GS, Jun JI, Cho DH, Choi HW, Lee HJ, et al. Inhibition of Bcl10-mediated activation of NF-kappa B by BinCARD, a Bcl10-interacting CARD protein. FEBS Lett. 2004; 578(3):239–44. https://doi.org/10.1016/j.febslet.2004.10.094 PMID: 15637807.

35. Subramanian N, Natarajan K, Clatworthy MR, Wang Z, Germain RN. The adaptor MAVS promotes NLRP3 mitochondrial localization and inflammasome activation. Cell. 2013; 153(2):348–61. https://doi.org/10.1016/j.cell.2013.02.054 PMID: 23582325.

36. Zhou R, Yazdi AS, Menu P, Tschopp J. A role for mitochondria in NLRP3 inflammasome activation. Nature. 2011; 469(7329):221–5. Epub 2010/12/03. https://doi.org/10.1038/nature09663 PMID: 21124315.

37. Mills EL, Kelly B, O'Neill LAJ. Mitochondria are the powerhouses of immunity. Nat Immunol. 2017; 18 (5):488–98. Epub 2017/04/19. https://doi.org/10.1038/ni.3704 PMID: 28418387.

38. Seth RB, Sun L, Ea C-K, Chen ZJ. Identification and Characterization of MAVS, a Mitochondrial Antiviral Signaling Protein that Activates NF-κB and IRF3. Cell. 2005; 122(5):669–82. https://doi.org/10.1016/j.cell.2005.08.012 PMID: 16125763

39. Elliott EI, Miller AN, Banoth B, Iyer SS, Stotland A, Weiss JP, et al. Cutting Edge: Mitochondrial Assembly of the NLRP3 Inflammasome Complex Is Initiated at Priming. The Journal of Immunology. 2018:ji1701723. https://doi.org/10.4049/jimmunol.1701723 PMID: 29602772

40. Carty M, Kearney J, Shanahan KA, Hams E, Sugisawa R, Connolly D, et al. Cell Survival and Cytokine Release after Inflammasome Activation Is Regulated by the Toll-IL-1R Protein SARM. Immunity. 2019; 50(6):1412–24.e6. Epub 2019/05/12. https://doi.org/10.1016/j.immuni.2019.04.005 PMID: 31076360.

41. Kayagaki N, Kornfeld OS, Lee BL, Stowe IB, O'Rourke K, Li Q, et al. NINJ1 mediates plasma membrane rupture during lytic cell death. Nature. 2021. https://doi.org/10.1038/s41586-021-03218-7 PMID: 33472215

42. Franchi L, Amer A, Body-Malapel M, Kanneganti TD, Ozoren N, Jagirdar R, et al. Cytosolic flagellin requires Ipaf for activation of caspase-1 and interleukin 1beta in *Salmonella*-infected macrophages. Nat Immunol. 2006; 7(6):576–82. Epub 2006/05/02. ni1346 [pii]. https://doi.org/10.1038/ni1346 PMID: 16648852.

43. Kofoed EM, Vance RE. Innate immune recognition of bacterial ligands by NAIPs determines inflammasome specificity. Nature. 2011; 477(7366):592–5. Epub 2011/08/30. https://doi.org/10.1038/nature10394 PMID: 21874021; PubMed Central PMCID: PMC3184209.

44. Mariathasan S, Weiss DS, Newton K, McBride J, O'Rourke K, Roose-Girma M, et al. Cryopyrin activates the inflammasome in response to toxins and ATP. Nature. 2006; 440(7081):228–32. Epub 2006/01/13. nature04515 [piihttps://doi.org/10.1038/nature04515 PMID: 16407890.

45. Munoz-Planillo R, Kuffa P, Martinez-Colon G, Smith BL, Rajendiran TM, Nunez G. K(+) efflux is the common trigger of NLRP3 inflammasome activation by bacterial toxins and particulate matter. Immunity. 2013; 38(6):1142–53. https://doi.org/10.1016/j.immuni.2013.05.016 PMID: 23809161; PubMed Central PMCID: PMC3730833.

46. Perregaux D, Gabel CA. Interleukin-1 beta maturation and release in response to ATP and nigericin. Evidence that potassium depletion mediated by these agents is a necessary and common feature of their activity. J Biol Chem. 1994; 269(21):15195–203. PMID: 8195155.

47. Solle M, Labasi J, Perregaux DG, Stam E, Petrushova N, Koller BH, et al. Altered cytokine production in mice lacking P2X(7) receptors. J Biol Chem. 2001; 276(1):125–32. https://doi.org/10.1074/jbc.M006781200 PMID: 11016935.

48. Sutterwala FS, Ogura Y, Szczepanik M, Lara-Tejero M, Lichtenberger GS, Grant EP, et al. Critical role for NALP3/CIAS1/Cryopyrin in innate and adaptive immunity through its regulation of caspase-1. Immunity. 2006; 24(3):317–27. Epub 2006/03/21. S1074-7613(06)00140-3 [pii]. https://doi.org/10.1016/j.immuni.2006.02.004 PMID: 16546100.

49. Philip NH, Dillon CP, Snyder AG, Fitzgerald P, Wynosky-Dolfi MA, Zwack EE, et al. Caspase-8 mediates caspase-1 processing and innate immune defense in response to bacterial blockade of NF-kappaB and MAPK signaling. Proceedings of the National Academy of Sciences of the United States of America. 2014; 111(20):7385–90. Epub 2014/05/07. https://doi.org/10.1073/pnas.1403252111 Epub 2014 May 5. PMID: 24799700; PubMed Central PMCID: PMC4034241.

50. Zhang Y, Ting AT, Marcu KB, Bliska JB. Inhibition of MAPK and NF-kappa B pathways is necessary for rapid apoptosis in macrophages infected with Yersinia. J Immunol. 2005; 174(12):7939–49. https://doi.org/10.4049/jimmunol.174.12.7939 PMID: 15944300.

51. Antonopoulos C, El Sanadi C, Kaiser WJ, Mocarski ES, Dubyak GR. Proapoptotic chemotherapeutic drugs induce noncanonical processing and release of IL-1beta via caspase-8 in dendritic cells. J Immunol. 2013; 191(9):4789–803. Epub 2013/10/01. https://doi.org/10.4049/jimmunol.1300645 Epub 2013 Sep 27. PMID: 24078693; PubMed Central PMCID: PMC3870469.

52. Bertrand R, Solary E, O'Connor P, Kohn KW, Pommier Y. Induction of a common pathway of apoptosis by staurosporine. Exp Cell Res. 1994; 211(2):314–21. https://doi.org/10.1006/excr.1994.1093 PMID: 8143779.

53. Jacobsen MD, Weil M, Raff MC. Role of Ced-3/ICE-family proteases in staurosporine-induced programmed cell death. J Cell Biol. 1996; 133(5):1041–51. https://doi.org/10.1083/jcb.133.5.1041 PMID: 8655577; PubMed Central PMCID: PMC2120856.

54. Degterev A, Hitomi J, Germscheid M, Ch'en IL, Korkina O, Teng X, et al. Identification of RIP1 kinase as a specific cellular target of necrostatins. Nat Chem Biol. 2008; 4(5):313–21. Epub 2008/04/15. https://doi.org/10.1038/nchembio.83 PMID: 18408713.

55. He S, Liang Y, Shao F, Wang X. Toll-like receptors activate programmed necrosis in macrophages through a receptor-interacting kinase-3-mediated pathway. Proceedings of the National Academy of Sciences of the United States of America. 2011; 108(50):20054–9. Epub 2011/11/30. https://doi.org/10.1073/pnas.1116302108 Epub 2011 Nov 28. PMID: 22123964; PubMed Central PMCID: PMC3250173.

56. Ghosn EEB, Cassado AA, Govoni GR, Fukuhara T, Yang Y, Monack DM, et al. Two physically, functionally, and developmentally distinct peritoneal macrophage subsets. Proceedings of the National Academy of Sciences. 2010; 107(6):2568. https://doi.org/10.1073/pnas.0915000107 PMID: 20133793

57. Okabe Y, Medzhitov R. Tissue-specific signals control reversible program of localization and functional polarization of macrophages. Cell. 2014; 157(4):832–44. Epub 2014/05/01. https://doi.org/10.1016/j.cell.2014.04.016 PMID: 24792964.

58. Bell CW, Jiang W, Reich CF, 3rd, Pisetsky DS. The extracellular release of HMGB1 during apoptotic cell death. Am J Physiol Cell Physiol. 2006; 291(6):C1318–25. https://doi.org/10.1152/ajpcell.00616.2005 PMID: 16855214.

59. Broz P, Dixit VM. Inflammasomes: mechanism of assembly, regulation and signalling. Nat Rev Immunol. 2016; 16(7):407–20. Epub 2016/06/14. https://doi.org/10.1038/nri.2016.58 PMID: 27291964.

60. Martinon F, Gaide O, Petrilli V, Mayor A, Tschopp J. NALP inflammasomes: a central role in innate immunity. Semin Immunopathol. 2007; 29(3):213–29. Epub 2007/08/19. https://doi.org/10.1007/s00281-007-0079-y PMID: 17703304.

61. Aglietti RA, Estevez A, Gupta A, Ramirez MG, Liu PS, Kayagaki N, et al. GsdmD p30 elicited by caspase-11 during pyroptosis forms pores in membranes. Proc Natl Acad Sci U S A. 2016; 113(28):7858–63. https://doi.org/10.1073/pnas.1607769113 PMID: 27339137; PubMed Central PMCID: PMC4948338.

62. Liu X, Zhang Z, Ruan J, Pan Y, Magupalli VG, Wu H, et al. Inflammasome-activated gasdermin D causes pyroptosis by forming membrane pores. Nature. 2016; 535(7610):153–8. https://doi.org/10.1038/nature18629 PMID: 27383986; PubMed Central PMCID: PMC5539988.

63. Kischkel FC, Hellbardt S, Behrmann I, Germer M, Pawlita M, Krammer PH, et al. Cytotoxicity-dependent APO-1 (Fas/CD95)-associated proteins form a death-inducing signaling complex (DISC) with the receptor. EMBO J. 1995; 14(22):5579–88. PMID: 8521815; PubMed Central PMCID: PMC394672.

64. Wallach D, Boldin M, Varfolomeev E, Beyaert R, Vandenabeele P, Fiers W. Cell death induction by receptors of the TNF family: towards a molecular understanding. FEBS Lett. 1997; 410(1):96–106. Epub 1997/06/23. https://doi.org/10.1016/s0014-5793(97)00553-x PMID: 9247131.

65. Denecker G, Declercq W, Geuijen CA, Boland A, Benabdillah R, van Gurp M, et al. Yersinia enterocolitica YopP-induced apoptosis of macrophages involves the apoptotic signaling cascade upstream of bid. J Biol Chem. 2001; 276(23):19706–14. https://doi.org/10.1074/jbc.M101573200 PMID: 11279213.

66. Li H, Zhu H, Xu CJ, Yuan J. Cleavage of BID by caspase 8 mediates the mitochondrial damage in the Fas pathway of apoptosis. Cell. 1998; 94(4):491–501. https://doi.org/10.1016/s0092-8674(00)81590-1 PMID: 9727492.

67. Rogers C, Fernandes-Alnemri T, Mayes L, Alnemri D, Cingolani G, Alnemri ES. Cleavage of DFNA5 by caspase-3 during apoptosis mediates progression to secondary necrotic/pyroptotic cell death. Nat Commun. 2017; 8:14128. https://doi.org/10.1038/ncomms14128 PMID: 28045099; PubMed Central PMCID: PMC5216131.

68. Bossaller L, Chiang PI, Schmidt-Lauber C, Ganesan S, Kaiser WJ, Rathinam VA, et al. Cutting edge: FAS (CD95) mediates noncanonical IL-1beta and IL-18 maturation via caspase-8 in an RIP3-independent manner. J Immunol. 2012; 189(12):5508–12. Epub 2012/11/13. https://doi.org/10.4049/jimmunol.1202121 Epub 2012 Nov 9. PMID: 23144495; PubMed Central PMCID: PMC3518757.

69. Conos SA, Lawlor KE, Vaux DL, Vince JE, Lindqvist LM. Cell death is not essential for caspase-1-mediated interleukin-1beta activation and secretion. Cell Death Differ. 2016; 23(11):1827–38. https://doi.org/10.1038/cdd.2016.69 PMID: 27419363; PubMed Central PMCID: PMC5071572.

70. Zwack EE, Feeley EM, Burton AR, Hu B, Yamamoto M, Kanneganti TD, et al. Guanylate Binding Proteins Regulate Inflammasome Activation in Response to Hyperinjected Yersinia Translocon Components. Infect Immun. 2017; 85(10). Epub 2017/08/09. https://doi.org/10.1128/IAI.00778-16 PMID: 28784930; PubMed Central PMCID: PMC5607426.

71. Zwack EE, Snyder AG, Wynosky-Dolfi MA, Ruthel G, Philip NH, Marketon MM, et al. Inflammasome activation in response to the Yersinia type III secretion system requires hyperinjection of translocon proteins YopB and YopD. MBio. 2015; 6(1):e02095–14. https://doi.org/10.1128/mBio.02095-14 PMID: 25691590; PubMed Central PMCID: PMC4337566.

72. Wolf AJ, Reyes CN, Liang W, Becker C, Shimada K, Wheeler ML, et al. Hexokinase Is an Innate Immune Receptor for the Detection of Bacterial Peptidoglycan. Cell. 2016; 166(3):624–36. https://doi.org/10.1016/j.cell.2016.05.076 Epub 2016 Jun 30. PMID: 27374331; PubMed Central PMCID: PMC5534359.

73. Wang Y, Shi P, Chen Q, Huang Z, Zou D, Zhang J, et al. Mitochondrial ROS promote macrophage pyroptosis by inducing GSDMD oxidation. Journal of Molecular Cell Biology. 2019; 11(12):1069–82. https://doi.org/10.1093/jmcb/mjz020 PMID: 30860577

74. Kim Y, Zhou P, Qian L, Chuang J-Z, Lee J, Li C, et al. MyD88-5 links mitochondria, microtubules, and JNK3 in neurons and regulates neuronal survival. The Journal of experimental medicine. 2007; 204 (9):2063–74. https://doi.org/10.1084/jem.20070868 PMID: 17724133.

75. Uccellini MB, Bardina SV, Sánchez-Aparicio MT, White KM, Hou Y-J, Lim JK, et al. Passenger Mutations Confound Phenotypes of SARM1-Deficient Mice. Cell reports. 2020; 31(1):107498. https://doi.org/10.1016/j.celrep.2020.03.062 PMID: 32268088.

76. Wang GG, Calvo KR, Pasillas MP, Sykes DB, Häcker H, Kamps MP. Quantitative production of macrophages or neutrophils ex vivo using conditional Hoxb8. Nature Methods. 2006; 3(4):287–93. https://doi.org/10.1038/nmeth865 PMID: 16554834

77. Purtha WE, Swiecki M, Colonna M, Diamond MS, Bhattacharya D. Spontaneous mutation of the Dock2 gene in Irf5<sup>−/−</

sup> mice complicates interpretation of type I interferon production and antibody responses. Proceedings of the National Academy of Sciences. 2012:201118155. https://doi.org/10.1073/pnas.1118155109 PMID: 22431588

78. Mahajan Vinay S, Demissie E, Mattoo H, Viswanadham V, Varki A, Morris R, et al. Striking Immune Phenotypes in Gene-Targeted Mice Are Driven by a Copy-Number Variant Originating from a Commercially Available C57BL/6 Strain. Cell Reports. 2016; 15(9):1901–9. https://doi.org/10.1016/j.celrep.2016.04.080 PMID: 27210752

79. Peterson LW, Philip NH, DeLaney A, Wynosky-Dolfi MA, Asklof K, Gray F, et al. RIPK1-dependent apoptosis bypasses pathogen blockade of innate signaling to promote immune defense. J Exp Med. 2017; 214(11):3171–82. https://doi.org/10.1084/jem.20170347 PMID: 28855241.

80. Weng D, Marty-Roix R, Ganesan S, Proulx MK, Vladimer GI, Kaiser WJ, et al. Caspase-8 and RIP kinases regulate bacteria-induced innate immune responses and cell death. Proceedings of the National Academy of Sciences of the United States of America. 2014; 111(20):7391–6. Epub 2014/05/07. https://doi.org/10.1073/pnas.1403477111 Epub 2014 May 5. PMID: 24799678; PubMed Central PMCID: PMC4034196.

81. Peterson LW, Philip NH, Dillon CP, Bertin J, Gough PJ, Green DR, et al. Cell-Extrinsic TNF Collaborates with TRIF Signaling To Promote Yersinia-Induced Apoptosis. J Immunol. 2016; 197(10):4110–7. https://doi.org/10.4049/jimmunol.1601294 PMID: 27733552; PubMed Central PMCID: PMC5123756.

82. Netea MG, Nold-Petry CA, Nold MF, Joosten LA, Opitz B, van der Meer JH, et al. Differential requirement for the activation of the inflammasome for processing and release of IL-1beta in monocytes and macrophages. Blood. 2009; 113(10):2324–35. https://doi.org/10.1182/blood-2008-03-146720 PMID: 19104081; PubMed Central PMCID: PMC2652374.

83. Pham CTN, MacIvor DM, Hug BA, Heusel JW, Ley TJ. Long-range disruption of gene expression by a selectable marker cassette. Proceedings of the National Academy of Sciences. 1996; 93(23):13090. https://doi.org/10.1073/pnas.93.23.13090 PMID: 8917549

84. Jin C, Kang H, Yoo T, Ryu JR, Yoo Y-E, Ma R, et al. The Neomycin Resistance Cassette in the Targeted Allele of Shank3B Knock-Out Mice Has Potential Off-Target Effects to Produce an Unusual Shank3 Isoform. Frontiers in Molecular Neuroscience. 2021; 13(245). https://doi.org/10.3389/fnmol.2020.614435 PMID: 33505245

85. West DB, Engelhard EK, Adkisson M, Nava AJ, Kirov JV, Cipollone A, et al. Transcriptome Analysis of Targeted Mouse Mutations Reveals the Topography of Local Changes in Gene Expression. PLOS Genetics. 2016; 12(2):e1005691. https://doi.org/10.1371/journal.pgen.1005691 PMID: 26839965

86. Evavold CL, Hafner-Bratkovič I, Devant P, D'Andrea JM, Ngwa EM, Boršić E, et al. Control of gasdermin D oligomerization and pyroptosis by the Ragulator-Rag-mTORC1 pathway. Cell. 2021; 184 (17):4495–511.e19. https://doi.org/10.1016/j.cell.2021.06.028 PMID: 34289345

87. Zheng Z, Deng W, Bai Y, Miao R, Mei S, Zhang Z, et al. The lysosomal Rag-Ragulator complex licenses RIPK1– and caspase-8–mediated pyroptosis by Yersinia. Science. 2021; 372(6549): eabg0269. https://doi.org/10.1126/science.abg0269

88. Rogers C, Erkes DA, Nardone A, Aplin AE, Fernandes-Alnemri T, Alnemri ES. Gasdermin pores permeabilize mitochondria to augment caspase-3 activation during apoptosis and inflammasome activation. Nature Communications. 2019; 10(1):1689. https://doi.org/10.1038/s41467-019-09397-2 PMID: 30976076

89. DeLaney AA, Berry CT, Christian DA, Hart A, Bjanes E, Wynosky-Dolfi MA, et al. Caspase-8 promotes c-Rel-dependent inflammatory cytokine expression and resistance against Toxoplasma gondii. Proc Natl Acad Sci U S A. 2019; 116(24):11926–35. Epub 20190530. https://doi.org/10.1073/pnas.1820529116 Epub 2019 May 30. PMID: 31147458; PubMed Central PMCID: PMC6575527.

90. Philip NH, DeLaney A, Peterson LW, Santos-Marrero M, Grier JT, Sun Y, et al. Activity of Uncleaved Caspase-8 Controls Anti-bacterial Immune Defense and TLR-Induced Cytokine Production Independent of Cell Death. PLoS Pathog. 2016; 12(10):e1005910. Epub 20161013. https://doi.org/10.1371/journal.ppat.1005910 eCollection 2016 Oct. PMID: 27737018; PubMed Central PMCID: PMC5063320.

91. Gitlin AD, Heger K, Schubert AF, Reja R, Yan D, Pham VC, et al. Integration of innate immune signalling by caspase-8 cleavage of N4BP1. Nature. 2020; 587(7833):275–80. Epub 20200924. https://doi.org/10.1038/s41586-020-2796-5 Epub 2020 Sep 24. PMID: 32971525.

92. Brodsky IE, Palm NW, Sadanand S, Ryndak MB, Sutterwala FS, Flavell RA, et al. A Yersinia effector protein promotes virulence by preventing inflammasome recognition of the type III secretion system. Cell Host Microbe. 2010; 7(5):376–87. Epub 2010/05/19. https://doi.org/10.1016/j.chom.2010.04.009 PMID: 20478539.

93. Szretter KJ, Daffis S, Patel J, Suthar MS, Klein RS, Gale M Jr., et al. The innate immune adaptor molecule MyD88 restricts West Nile virus replication and spread in neurons of the central nervous system.

J Virol. 2010; 84(23):12125–38. Epub 2010/10/01. https://doi.org/10.1128/JVI.01026-10 Epub 2010 Sep 29. PMID: 20881045; PubMed Central PMCID: PMC2976388.

94. Rauch I, Deets KA, Ji DX, von Moltke J, Tenthorey JL, Lee AY, et al. NAIP-NLRC4 Inflammasomes Coordinate Intestinal Epithelial Cell Expulsion with Eicosanoid and IL-18 Release via Activation of Caspase-1 and -8. Immunity. 2017; 46(4):649–59. https://doi.org/10.1016/j.immuni.2017.03.016 PMID: 28410991; PubMed Central PMCID: PMC5476318.

95. Newton K, Sun X, Dixit VM. Kinase RIP3 is dispensable for normal NF-kappa Bs, signaling by the B-cell and T-cell receptors, tumor necrosis factor receptor 1, and Toll-like receptors 2 and 4. Mol Cell Biol. 2004; 24(4):1464–9. https://doi.org/10.1128/MCB.24.4.1464-1469.2004 PMID: 14749364; PubMed Central PMCID: PMC344190.

96. Oberst A, Dillon CP, Weinlich R, McCormick LL, Fitzgerald P, Pop C, et al. Catalytic activity of the caspase-8-FLIP(L) complex inhibits RIPK3-dependent necrosis. Nature. 2011; 471(7338):363–7. Epub 2011/03/04. https://doi.org/10.1038/nature09852 Epub 2011 Mar 2. PMID: 21368763; PubMed Central PMCID: PMC3077893.

97. Wang S, Miura M, Jung YK, Zhu H, Li E, Yuan J. Murine caspase-11, an ICE-interacting protease, is essential for the activation of ICE. Cell. 1998; 92(4):501–9. https://doi.org/10.1016/s0092-8674(00)80943-5 PMID: 9491891.

98. Bray NL, Pimentel H, Melsted P, Pachter L. Near-optimal probabilistic RNA-seq quantification. Nat Biotechnol. 2016; 34(5):525–7. https://doi.org/10.1038/nbt.3519 PMID: 27043002.

99. Huber W, Carey VJ, Gentleman R, Anders S, Carlson M, Carvalho BS, et al. Orchestrating high-throughput genomic analysis with Bioconductor. Nature Methods. 2015; 12(2):115–21. https://doi.org/10.1038/nmeth.3252 PMID: 25633503

100. Soneson C, Love MI, Robinson MD. Differential analyses for RNA-seq: transcript-level estimates improve gene-level inferences. F1000Research. 2015; 4:1521. Epub 2016/03/01. https://doi.org/10.12688/f1000research.7563.2 PMID: 26925227; PubMed Central PMCID: PMC4712774.

101. Robinson MD, McCarthy DJ, Smyth GK. edgeR: a Bioconductor package for differential expression analysis of digital gene expression data. Bioinformatics. 2010; 26(1):139–40. Epub 2009/11/17. https://doi.org/10.1093/bioinformatics/btp616 PMID: 19910308; PubMed Central PMCID: PMC2796818.

102. Ritchie ME, Phipson B, Wu D, Hu Y, Law CW, Shi W, et al. limma powers differential expression analyses for RNA-sequencing and microarray studies. Nucleic Acids Res. 2015; 43(7):e47. https://doi.org/10.1093/nar/gkv007 Epub 2015 Jan 20. PMID: 25605792; PubMed Central PMCID: PMC4402510.

103. EnhancedVolcano: Publication-ready volcano plots with enhanced colouring and labeling. [Internet]. 2018. Available from: https://github.com/kevinblighe/EnhancedVolcano.